NASA/TP-1998-206544

Development of the X-33 Aerodynamic Uncertainty Model

Brent R. Cobleigh
Dryden Flight Research Center
Edwards, California

National Aeronautics and
Space Administration

Dryden Flight Research Center
Edwards, California 93523-0273

April 1998

NOTICE

Use of trade names or names of manufacturers in this document does not constitute an official endorsement of such products or manufacturers, either expressed or implied, by the National Aeronautics and Space Administration.

Available from the following:

NASA Center for AeroSpace Information (CASI)
7121 Standard Drive
Hanover, MD 21076-1320
(301) 621-0390

National Technical Information Service (NTIS)
5285 Port Royal Road
Springfield, VA 22161-2171
(703) 487-4650

ABSTRACT

An aerodynamic uncertainty model for the X-33 single-stage-to-orbit demonstrator aircraft has been developed at NASA Dryden Flight Research Center. The model is based on comparisons of historical flight test estimates to preflight wind-tunnel and analysis code predictions of vehicle aerodynamics documented during six lifting-body aircraft and the Space Shuttle Orbiter flight programs. The lifting-body and Orbiter data were used to define an appropriate uncertainty magnitude in the subsonic and supersonic flight regions, and the Orbiter data were used to extend the database to hypersonic Mach numbers. The uncertainty data consist of increments or percentage variations in the important aerodynamic coefficients and derivatives as a function of Mach number along a nominal trajectory. The uncertainty models will be used to perform linear analysis of the X-33 flight control system and Monte Carlo mission simulation studies. Because the X-33 aerodynamic uncertainty model was developed exclusively using historical data rather than X-33 specific characteristics, the model may be useful for other lifting-body studies.

NOMENCLATURE

b	reference span, ft
BF	body flap, deg
C_D	drag coefficient
$C_{D_{nom}}$	nominal drag coefficient
C_l	rolling moment coefficient
C_{l_p}	derivative of rolling moment due to nondimensional roll rate, $\partial C_l/\partial(pb/2V)$, rad^{-1}
C_{l_r}	derivative of rolling moment due to nondimensional yaw rate, $\partial C_l/\partial(rb/2V)$, rad^{-1}
C_{l_β}	derivative of rolling moment due to sideslip, $\partial C_l/\partial\beta$, deg^{-1}
$C_{l_{\delta a}}$	derivative of rolling moment due to aileron, $\partial C_l/\partial\delta a$, deg^{-1}
$C_{l_{\delta r}}$	derivative of rolling moment due to rudder, $\partial C_l/\partial\delta r$, deg^{-1}
C_L	lift coefficient
$C_{L_{nom}}$	nominal lift coefficient
C_m	pitching moment coefficient
C_{m_q}	derivative of pitching moment due to nondimensional pitch rate, $\partial C_m/\partial(qL/2V)$, rad^{-1}
$C_{m_{\delta bf}}$	derivative of pitching moment due to body flap, $\partial C_m/\partial\delta bf$, deg^{-1}
$C_{m_{\delta e}}$	derivative of pitching moment due to elevon, $\partial C_m/\partial\delta e$, deg^{-1}
C_n	yawing moment coefficient
C_{n_p}	derivative of yawing moment due to nondimensional roll rate, $\partial C_n/\partial(pb/2V)$, rad^{-1}
C_{n_r}	derivative of yawing moment due to nondimensional yaw rate, $\partial C_n/\partial(rb/2V)$, rad^{-1}
C_{n_β}	derivative of yawing moment due to sideslip, $\partial C_n/\partial\beta$, deg^{-1}
$C_{n_{\delta a}}$	derivative of yawing moment due to aileron, $\partial C_n/\partial\delta a$, deg^{-1}

$C_{n_{\delta r}}$	derivative of yawing moment due to rudder, $\partial C_n/\partial \delta r$, deg^{-1}
C_Y	side force coefficient
C_{Y_β}	derivative of side force due to sideslip, $\partial C_Y/\partial \beta$, deg^{-1}
$C_{Y_{\delta a}}$	derivative of side force due to aileron, $\partial C_Y/\partial \delta a$, deg^{-1}
$C_{Y_{\delta r}}$	derivative of side force due to rudder, $\partial C_Y/\partial \delta r$, deg^{-1}
FAD	flight assessment delta
L	vehicle reference length, ft
L/D	lift-to-drag ratio
L/D_{nom}	nominal lift-to-drag ratio
L/D_{unc}	lift-to-drag ratio uncertainty
MAC	mean aerodynamic chord
p	roll rate, rad/sec
q	pitch rate, rad/sec
r	yaw rate, rad/sec
RCS	reaction control system
V	velocity, ft/sec
α	angle of attack, deg
β	angle of sideslip, deg
δa	aileron deflection, deg
δbf	body flap deflection, deg
δe	elevon deflection, deg
δr	rudder deflection, deg
Δ	increment from nominal
ΔC_D	modified drag uncertainty
$\Delta C_{D_{unc}}$	unmodified drag uncertainty
ΔC_L	modified lift uncertainty
$\Delta C_{L_{unc}}$	unmodified lift uncertainty
σ	standard deviation

INTRODUCTION

Part of the design and implementation of any control system involves the testing for potential errors, also called uncertainties or dispersions, in the mathematical model of the system and in any inputs used by the control algorithms. Some of the uncertainties, such as the accuracy of a particular instrument, can be measured through laboratory testing; however, errors in the system model are frequently not easily measurable or are excessively expensive to obtain. In these cases, engineering judgment is often used to

construct an uncertainty model of the system that will allow for adequate "stress" testing of the proposed control algorithms. If the model is too severe, the system may be found to be uncontrollable or the performance of the system may be unduly penalized. Errors that are not modeled adequately can result in a system that is unable to handle reasonable variances or failures. For traditional piloted vehicles, the control system is stress-tested to a reasonable degree, assuming that any remaining handling anomalies should be compensable by the pilot. Autonomous vehicles, however, do not have the luxury of a pilot and, therefore, must be designed to handle any "reasonable" error in the system model.

One of the most detailed analyses into aerodynamic uncertainty modeling was completed for the Space Shuttle Orbiter program.[1] The Orbiter aerodynamic uncertainty model consisted of two parts. The first part was based on the wind tunnel–to–wind tunnel and model-to-model variations gathered during the 27,000-hour wind-tunnel test program that was used to derive the aerodynamic model. These deviations, termed "tolerances," were considered to be the minimum error that should be expected. The control laws would need to be able to handle these errors with little or no effect on the vehicle stability or guidance. The second part of the uncertainty model was based on the differences between the historical flight test measurements and the preflight predictions found for many similar (in configuration or mission) vehicles.[2] By combining as many similar vehicles as possible, a pseudo "worst-case" aerodynamic prediction error bound was estimated for each of the important aerodynamic coefficients. These worst-case aerodynamic uncertainties were termed "variations."

This paper addresses the development of the initial aerodynamic uncertainty models for the X-33 single-stage-to-orbit technology demonstrator. The uncertainties are based on comparisons between historical flight measurements and preflight predictions of other similar aircraft configurations. In most cases, the preflight predictions were based on wind-tunnel data, although some prediction code data were used. The uncertainties are analogous to the variations developed during the Orbiter program. These uncertainties provide the basis for "stress" testing of candidate X-33 guidance and control systems. The stress testing will consist of linear analysis at selected flight conditions and complete mission Monte Carlo simulations. In this way, both the vehicle closed-loop control and the vehicle guidance control law will be tested. Further refinement of the X-33 aerodynamic uncertainty model may occur as the wind-tunnel test program is completed. Flight test validation of the wind-tunnel database will likely reduce the uncertainty. This report describes the vehicles used to build the aerodynamic uncertainty models, details the method used to gather data, and presents the uncertainty models selected for the X-33 program. The appropriate use of the models is also discussed.

VEHICLE DESCRIPTIONS

The X-33 aircraft (fig. 1) is an autonomous, hypersonic, lifting-body-type demonstrator vehicle designed to validate the technologies necessary for a single-stage-to-orbit reusable launch vehicle. The vehicle uses linear aerospike rocket engines capable of thrust vectoring in pitch, roll, and yaw. In addition to thrust vectoring, the vehicle uses lower, outboard body flaps for pitch, roll, and yaw control; two rudders symmetrically for low angle-of-attack yaw control and asymmetrically for energy management and pitch control; and two small, 20° dihedral wings with trailing-edge elevon flaps that produce pitch, roll, and yaw. Eight aft-mounted reaction control system (RCS) jets are also available for high-speed, high-altitude control.

The M2-F1 aircraft (fig. 2(a)) was a lightweight glider designed for subsonic investigations of the lifting-body concept. Longitudinal control was provided by an upper body flap and elevons, located on

the upper, outboard rudder surface. Roll control came from differential deflection of the elevons and directional control from the two vertical rudders.

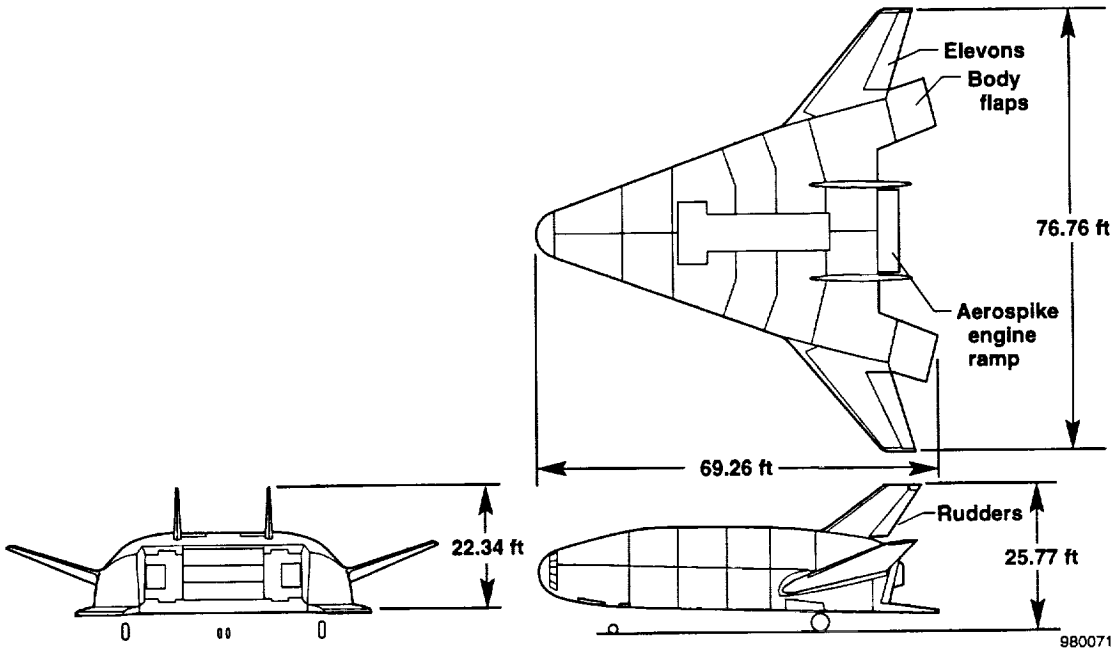

Figure 1. Three-view of the X-33 vehicle.

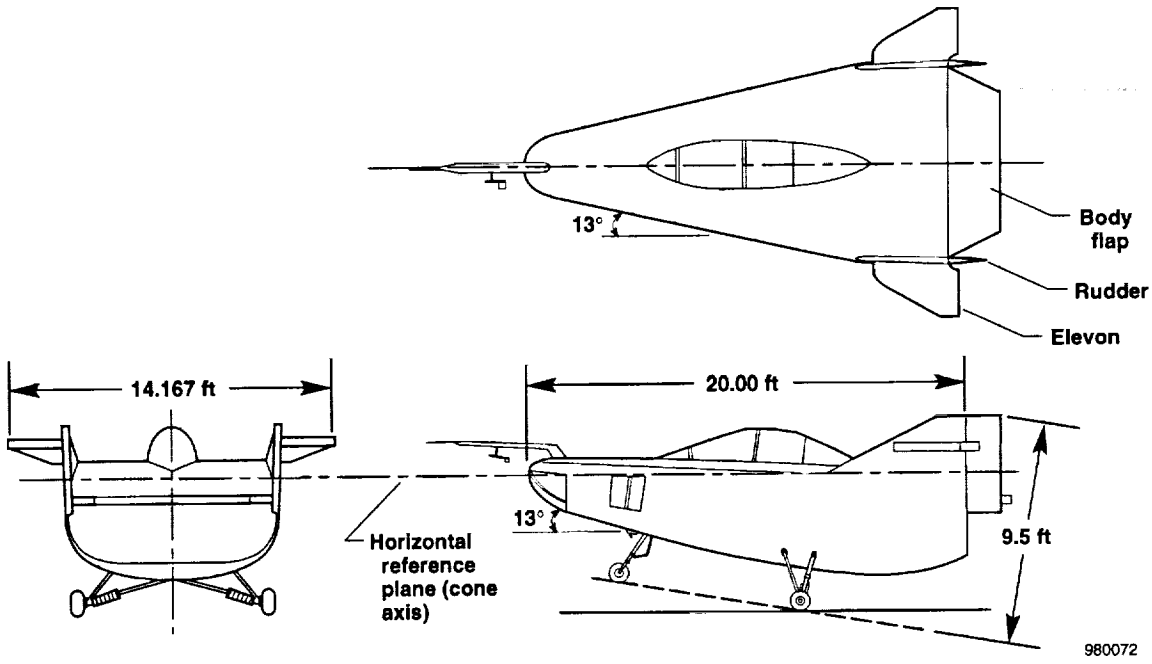

(a) The M2-F1 vehicle.

Figure 2. Three-view drawing of vehicles used to develop the X-33 aerodynamic uncertainty model.

The M2-F2 aircraft (fig. 2(b)) was a rocket-powered, blunt, 13°-half-cone-shaped lifting-body vehicle. The vehicle had two outboard fins that had rudder surfaces that could only deflect outward. Primary pitch control was provided by a lower body flap, and roll control came from the two upper body flaps.

The M2-F3 aircraft (fig. 2(c)) was a slight variation on the M2-F2 configuration. An additional vertical fin was added between the upper flaps. The design also included a rocket engine for higher speed and longer duration flights than the M2-F2 aircraft achieved.

The HL-10 aircraft (fig. 2(d)) was a rocket-powered, negative-camber lifting body designed to test at subsonic to low supersonic Mach numbers. Elevons were used as the primary longitudinal and roll control effectors. Directional control came from the rudder located on the center, vertical fin. Two other slightly canted-out fins were located outboard. Surfaces on the outboard fins and an upper flap on each of the elevons were used to adjust the vehicle configuration.

The X-24A aircraft (fig. 2(e)) was another rocket-powered, lifting-body research vehicle. The aircraft had three vertical fins: one along the centerline and two slightly canted out, outboard. Each of the outboard fins had an upper and lower rudder surface. For pitch and roll control, two upper and two lower flaps were included.

The X-24B aircraft (fig. 2(f)) had a double-delta planform with a flat bottom and flat sides. The upper surface was a curved airfoil with three vertical fins. The off-center fins were located inboard of the wingtips and canted out. The aerodynamic control surfaces included two upper and two lower flaps, two upper and two lower rudders, and two ailerons. The lower flaps provided the primary pitch control.

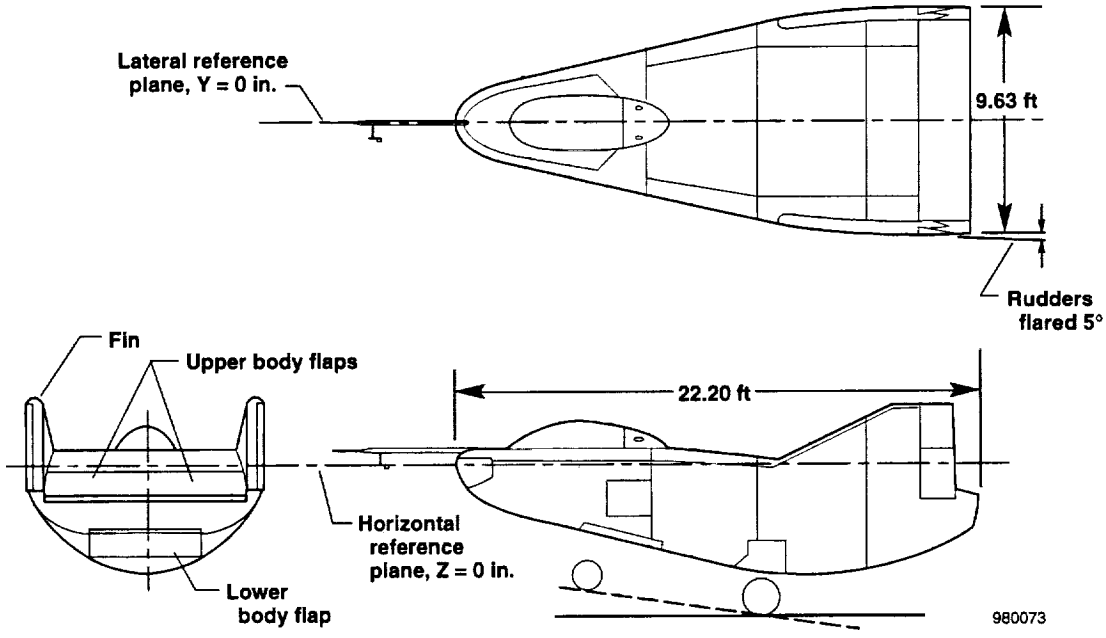

(b) The M2-F2 vehicle.

Figure 2. Continued.

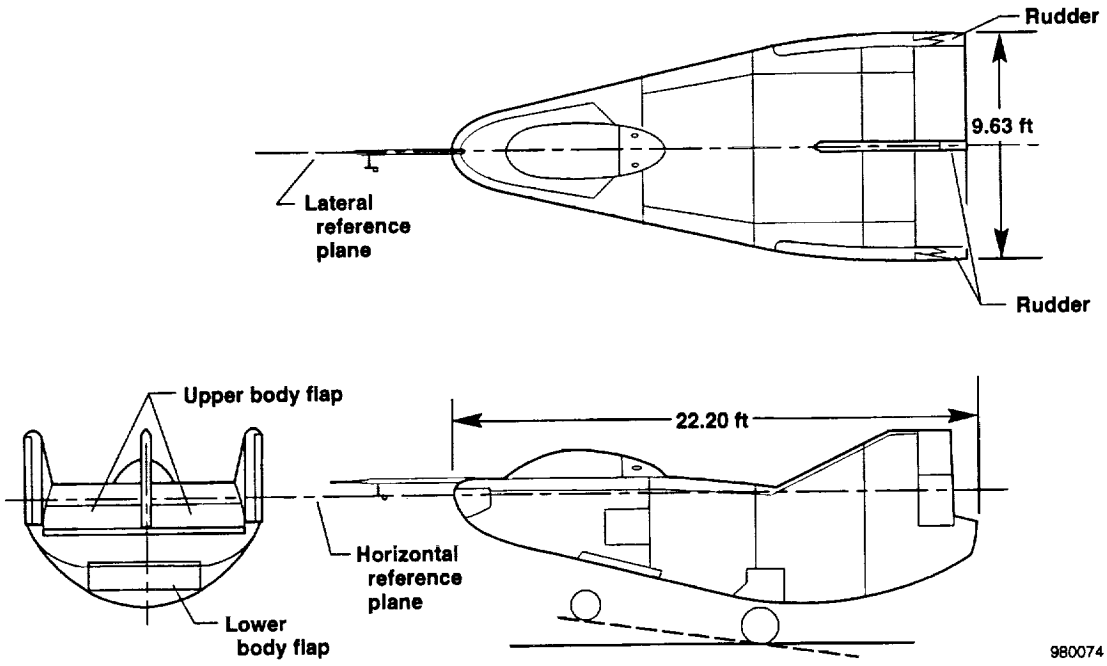

(c) The M2-F3 vehicle.

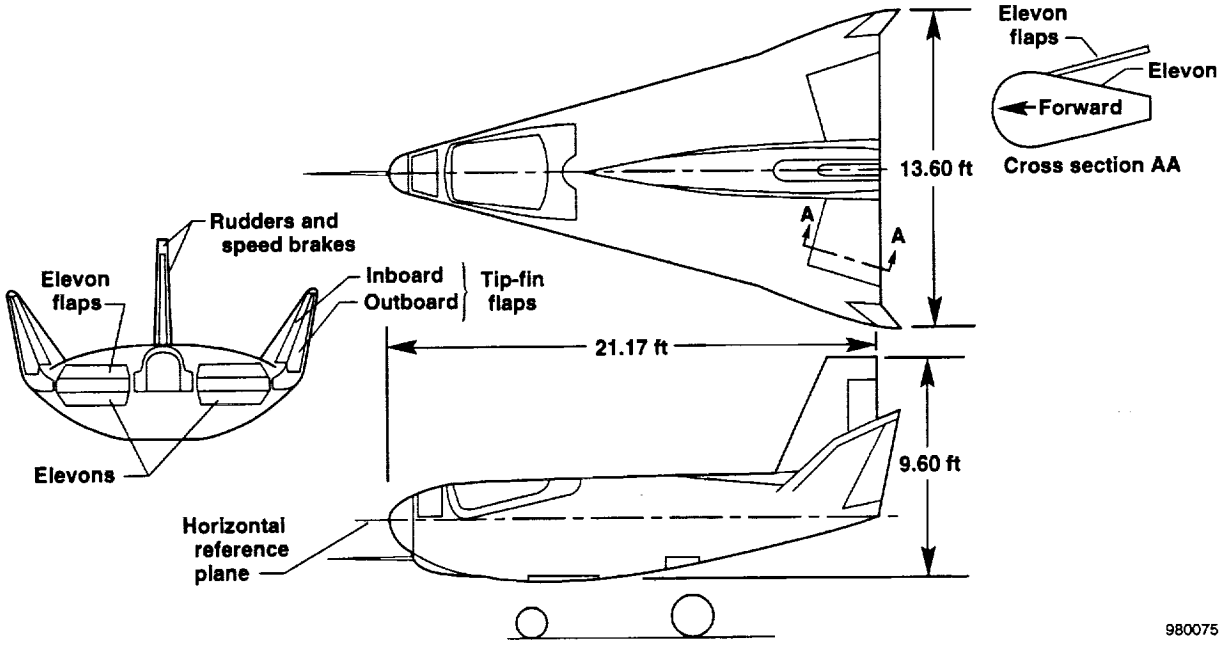

(d) The HL-10 vehicle.

Figure 2. Continued.

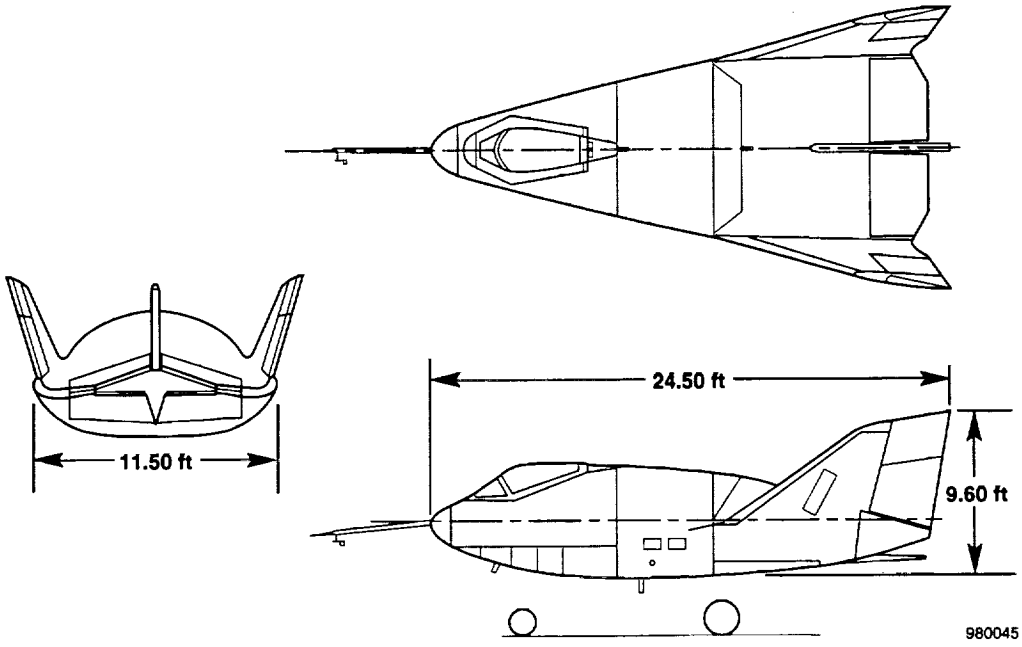

(e) The X-24A vehicle.

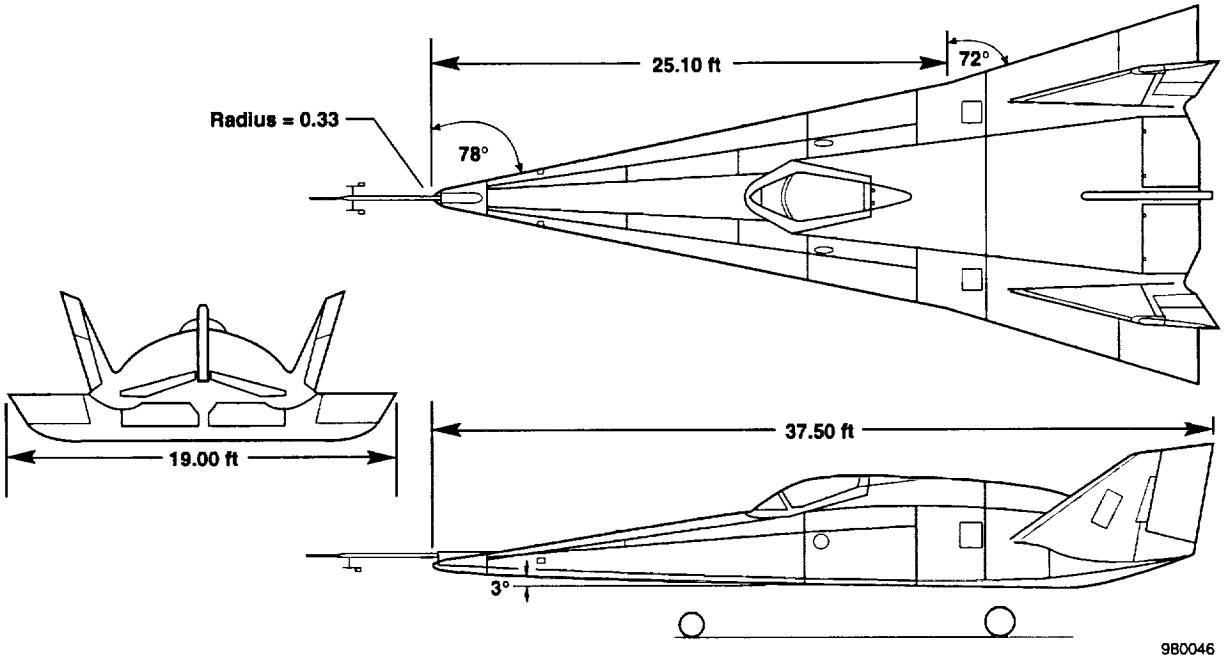

(f) The X-24B vehicle.

Figure 2. Continued.

The Space Shuttle Orbiter (fig. 2(g)) is a large, double-delta-winged vehicle designed to enter the atmosphere and land horizontally. Control power for Orbiter reentry is provided by 12 vertical RCS jets (6 down-firing and 6 up-firing), 8 horizontal RCS jets (4 to the left and 4 to the right), 4 wing-mounted elevon surfaces, a lower body flap, and a split rudder surface. Used symmetrically, the vertical jets and the elevons are the primary controls for the pitch axis. Roll control is obtained through asymmetrical usage of the vertical jets and elevons. Used as a secondary pitch trim control, the body flap helps maintain the predetermined elevon schedule as a function of flight condition. The rudder and the side firing jets provide the directional control. The body flap and elevons activate at a dynamic pressure of 2 lbf/ft^2. The rudders activate at Mach numbers below 5.

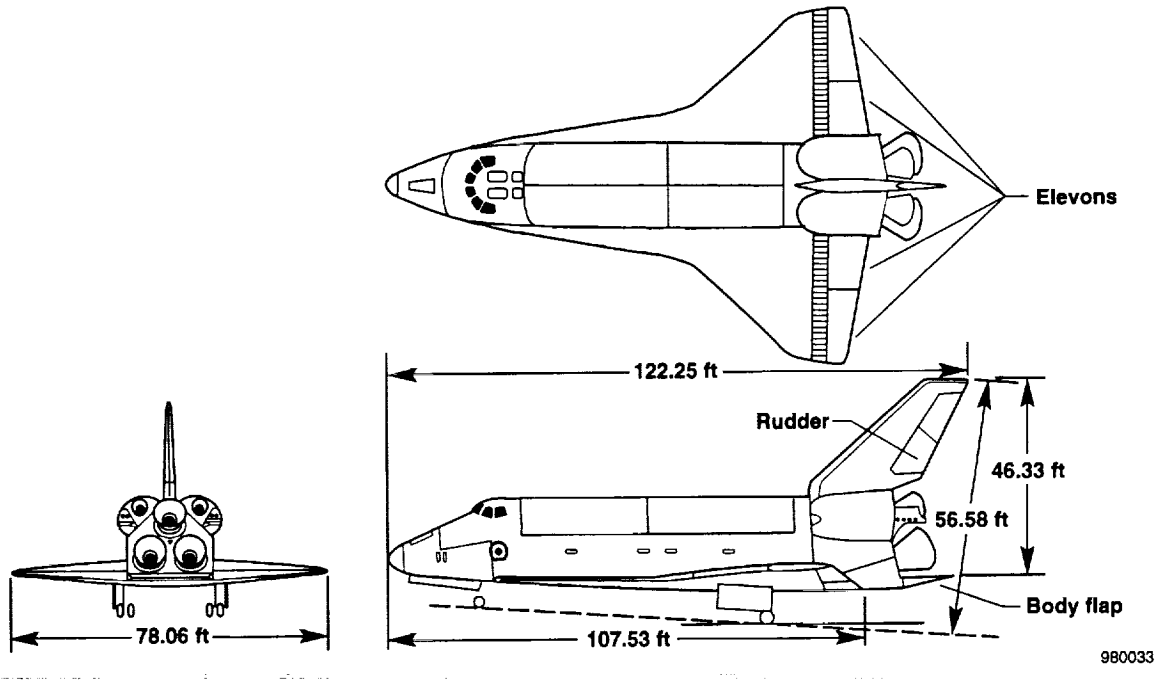

(g) The Space Shuttle Orbiter.

Figure 2. Concluded.

METHOD

The development of an appropriate uncertainty model for the X-33 aerodynamics began with a review of the historical flight test documentation of similar vehicle configuration. By comparing the flight test–measured aerodynamics to wind-tunnel measurements or engineering code estimates of other similar vehicles, a database of actual prediction errors was generated. This database was used as a guide in determining an appropriate uncertainty magnitude for each of the important aerodynamic parameters as a function of flight condition. Table 1 shows a list of the vehicles used in the study and some geometric data. The lifting-body configurations (the HL-10, M2-F1, M2-F2, M2-F3, X-24A, and X-24B aircraft) were chosen because of their geometric similarity to the X-33 vehicle and the availability of acceptable documentation. The Orbiter was also selected for its largely similar angle-of-attack and Mach number mission profile and its excellent flight-to-preflight prediction documentation. The flight and preflight

data used in the study were obtained from previous publications.[3–15] The following subsections describe how the X-33 aerodynamic uncertainty model was developed from the lifting-body and Orbiter databases.

Table 1. Vehicles with basic geometry.

Vehicle	Area, ft^2	Length, ft	Span, ft	Sweep, deg
M2-F1	139.0 actual	20.00 actual	9.50 actual	77.0
M2-F2	139.0 reference 160.0 actual	20.00 reference 22.20 actual	9.54 reference 9.63 actual	77.0
M2-F3	160.0 reference 156.0 actual	22.20 actual	9.95 reference 9.63 actual	77.0
HL-10	160.0 reference	21.17 reference	13.60 reference	74.0
X-24A	162.0 reference 195.0 actual	23.00 reference	10.00 reference	75.0
X-24B	330.5 reference	37.50 reference	19.00 reference 19.17 actual	78.0 inboard 72.0 outboard
Orbiter	2690.0 reference	108.03 body 39.56 MAC (ref.)	78.06 reference	81.0 strake 45.0 wing
X-33	1608.0 reference	63.20 reference	36.60 reference	70.0

Lifting Body Aerodynamic Uncertainties

Engineering judgment was used in the selection of the lifting-body data for this model. The postflight aerodynamic estimates were subject to several error sources such as an inadequate number of flight test maneuvers, instrument measurement errors, and immature prediction techniques. Using the aforementioned reasoning, much of the HL-10 damping, M2-F1 lateral, M2-F3 longitudinal, and X-24A longitudinal data were not used in the study.

Figure 3 shows the process used to obtain the static stability and control derivative uncertainty data. The flight-measured aerodynamic parameter estimates were plotted as a function of angle of attack at a given Mach number, and a fairing was drawn through the points based on engineering judgment. The fairing helps to reduce variations in the estimates that are caused by maneuver quality and analysis variations. Because all parameter estimation codes are statistically based, the analysis of several maneuvers at the same flight condition is a common practice to reduce maneuver, instrumentation, and analysis variations. The differences between the flight fairing and preflight predictions were calculated. Usually data were taken in 4° angle-of-attack increments (for example, 0°, 4°, 8°).

To minimize the effects of varying planform layout, the data were compiled as a percentage of the prediction where possible.

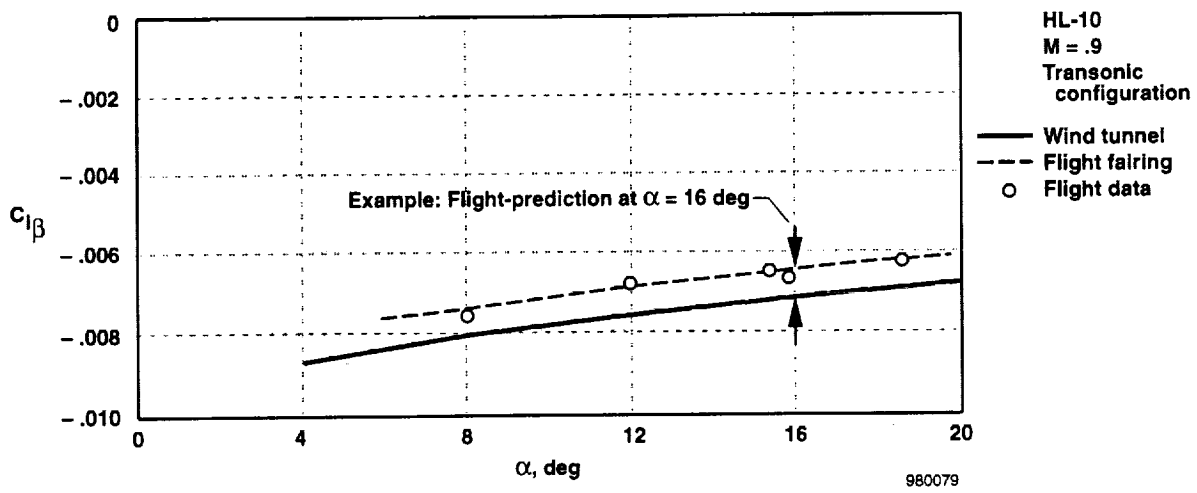

Figure 3. Example of data gathering method.

$$\text{(Method 1)} \qquad \text{uncertainty (percent)} = \frac{(\text{flight} - \text{prediction})}{\text{prediction}} \times 100$$

The percentage data format was used for the $C_{l_{\delta a}}$, $C_{n_{\delta r}}$, $C_{m_{\delta bf}}$, $C_{m_{\delta e}}$, C_{m_q}, C_{l_p}, C_{l_r}, C_{n_p}, and C_{n_r} derivatives. Parameters that had small magnitudes or changed signs somewhere in the flight envelope were not good candidates for presenting the uncertainties in a percentage format. As a result, many of the aerodynamic parameters are presented as an increment from the prediction.

(Method 2) uncertainty (increment) = flight – prediction

This method was done for the C_L, C_D, C_m, and L/D coefficients and the C_{Y_β}, C_{l_β}, C_{n_β}, $C_{Y_{\delta a}}$, $C_{n_{\delta a}}$, $C_{Y_{\delta r}}$, and $C_{l_{\delta r}}$ derivatives.

In general, the rotary derivatives had a larger amount of variation than the rest of the parameters, making it difficult to select a flight-estimated value that would summarize the data. The data points from each individual maneuver (rather than a fairing of the data) were compared to the preflight estimate. As a result, additional scatter in uncertainty data would be expected. Originally, the damping derivative uncertainty data were collected in incremental format as shown in method 2. A comparison of the reasonable maximum increment values to the X-33 rotary derivatives yielded cases where the primary rotary derivatives (C_{l_p}, C_{n_r}, and C_{m_q}) would be unstable. Because this prediction seemed to be excessively pessimistic for this type of vehicle, the data were reevaluated using method 1.

Individual lifting-body flight test–measured damping derivatives were found to retain, in general, a minimum of 50 percent of the damping of the preflight estimate. The flight data also showed increased damping in approximately 50 percent of the data.

Orbiter Aerodynamic Uncertainties

The Orbiter aerodynamic database has been derived from an enormous wind-tunnel test program. This level of effort will not be expended to develop the X-33 aerodynamic database, or likely any other future database. In terms of wind-tunnel testing, the Orbiter has perhaps the best preflight wind-tunnel prediction that can be expected. In addition, a team of highly experienced engineers has been involved in updating the Orbiter aerodynamic database using the latest analysis techniques.

The Orbiter preflight aerodynamic database has been supplemented with flight assessment deltas (FADs), which are increments between the flight test and preflight aerodynamic predictions. Thus, the FADs represent the error in the Orbiter preflight database as found in flight test. These increments are used directly in this study. In addition to the FADs, the Orbiter program used aerodynamic uncertainties (originally developed in a similar fashion to this study) that have been modified using flight predictions. These uncertainties were also used in this work to develop the X-33 aerodynamic uncertainties. Because the Orbiter aerodynamic database was developed from such an extensive ground test program, its uncertainty levels would, in general, be smaller than those expected for the X-33 aircraft.

All of the lifting-body programs, including the X-33 program, use the body length as the reference length to nondimensionalize the pitching moment coefficient. The Orbiter uses the wing mean aerodynamic chord. To ensure a correct comparison, the Orbiter pitching moment coefficients were multiplied by the ratio of the Orbiter wing mean aerodynamic chord to the Orbiter body length.

The Orbiter FADs and uncertainties are documented as a function of Mach number and, in some cases, elevon or body flap position around the scheduled angle of attack. Both the FAD and Orbiter uncertainty databases are valid to a maximum 10° angle-of-attack deviation from the nominal schedule. Figure 4 shows a comparison between the Orbiter and three X-33 trajectories. For all planned trajectories, the X-33 angle-of-attack schedule is within 10° of the Orbiter nominal trajectory during the reentry portion of the flight. During the other phases of the trajectory, the X-33 angle of attack is lower than the Orbiter angle of attack for a given Mach number. Assuming that the uncertainties generally increase with increasing angle of attack, using the reentry schedule uncertainties during other phases of the flight should be a conservative approach.

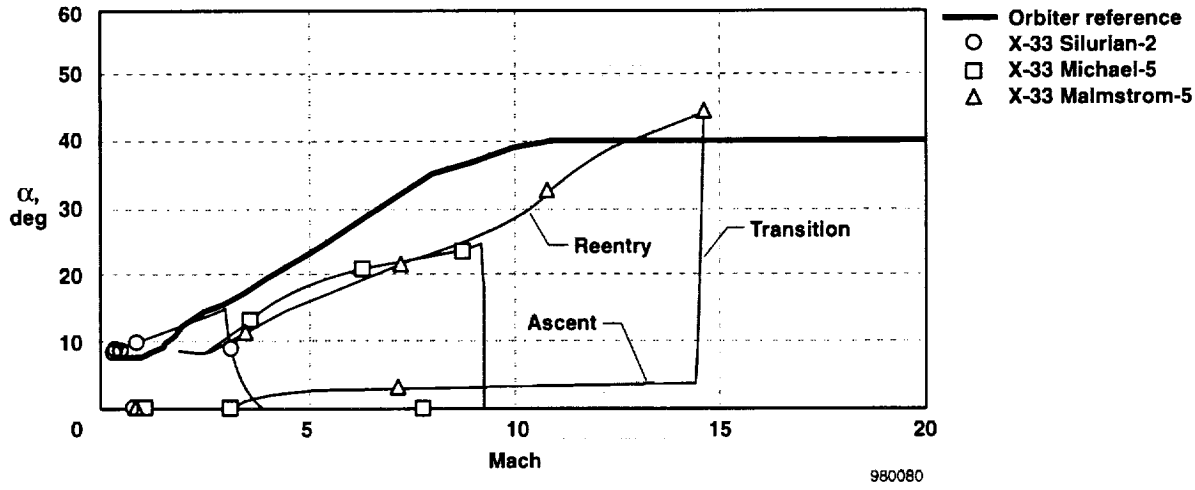

Figure 4. Comparison of X-33 and Space Shuttle Orbiter reentry trajectories.

X-33 Aerodynamic Uncertainty Model

The coefficient uncertainty data described in the previous sections were combined and plotted as a function of Mach number for each of the coefficients and derivatives. When plotted, a judgment on the maximum expected uncertainties in the predicted parameters was made. Where data were sparse, the Orbiter uncertainty was used to help define the shape of the X-33 aerodynamic uncertainty, particularly at high supersonic Mach numbers where no lifting-body data exist. An explanation of the development of each coefficient uncertainty is given in the next section.

The aerodynamic uncertainties generated in this work do not attempt to account for structural flexibility. The uncertainties should be applied to the rigid-body aerodynamics before the flexibility corrections are applied.

Note that the preceding method for developing the X-33 uncertainty model did not depend on any particular X-33 characteristic other than its generic lifting-body-type shape. Thus, the database may be useful for other lifting-body studies.

UNCERTAINTY MODEL DEVELOPMENT

The data for the important aerodynamic parameters and a suggested X-33 uncertainty model are presented in this section. Data were available from six lifting-body configurations (the HL-10, M2-F1, M2-F2, M2-F3, X-24A, and X-24B vehicles) to a maximum of Mach 1.6 and from the Orbiter to Mach 30. Angle-of-attack variations do not directly show up in the model, although the Mach number data includes the effect of the nominal trim angle of attack.

Longitudinal Uncertainties

The X-33 drag, lift, pitching moment, longitudinal control effectiveness, and pitching moment due to pitch rate uncertainties are discussed in this subsection. A method to limit the maximum lift and drag ratio uncertainties to prevent an unrealistic lift-to-drag ratio uncertainty is also presented.

Drag

For a variety of reasons (including sting, Reynolds number, real gas and tunnel blockage effects), drag is susceptible to errors during wind-tunnel testing. This susceptibility is evident in the flight-to-prediction comparisons for the Orbiter (fig. 5(a)). The drag coefficient prediction is incorrect by as much as 100 counts to –200 counts transonically. At subsonic and low supersonic Mach numbers, the Orbiter angle of attack is less than 15°. At Mach numbers greater than 5, the drag error increases. Explanations for the increasing drag uncertainty include increasing errors in the induced drag at increasing angle of attack, and difficulties in reproducing the hypersonic Reynold's number and real gas environments in a wind tunnel. As shown in figure 2, the Orbiter angle of attack is greater than 25° when the Mach number is greater than 5. The lifting-body results show positive and negative drag increments that are generally bounded by the Orbiter uncertainty boundaries. Both the X-24B and Orbiter data have sharp negative and then positive peaks in the drag increment near Mach 1.0. This fluctuation is likely caused by a misprediction of the Mach number at which the transonic drag rise occurs, a common problem caused by wind-tunnel blockage effects. Because the X-33 vehicle will have a limited wind-tunnel test program and its base area is responsible for more than 80 percent of its total zero-lift drag, the X-33 drag prediction is

more susceptible to wind-tunnel errors than most predications. A recommended X-33 drag coefficient uncertainty—chosen slightly larger in the transonic region than the Orbiter uncertainty—is plotted in figure 5(a) and tabulated in table 2.

Table 2. The X-33 lift, drag, and L/D uncertainty model.

Mach	ΔC_L	ΔC_D	$\Delta L/D$
0.10	0.050	0.0125	0.2700
0.40			0.2700
0.50		0.0125	0.2950
0.60			0.3120
0.70		0.0225	0.3000
0.80			0.2860
0.90			0.2640
0.95			0.2340
0.98			0.2160
1.00			0.2050
1.10			0.1800
1.20		0.0225	
1.25			0.1680
1.50		0.0150	0.1560
1.75			0.1470
2.00			0.1420
3.00	0.050	0.0150	0.1120
5.00			0.0864
6.00		0.0400	
10.00			0.0480
11.00	0.075		
15.00			0.0480
16.00			0.0340
20.00		0.0400	
30.00	0.075	0.0600	0.0340

Lift

Figure 5(b) shows a limited amount of lift coefficient prediction error data. Historically, lift is reasonably well-predicted in the wind tunnel. The recommended X-33 lift coefficient uncertainty is shown in figure 5(b) and tabulated in table 2.

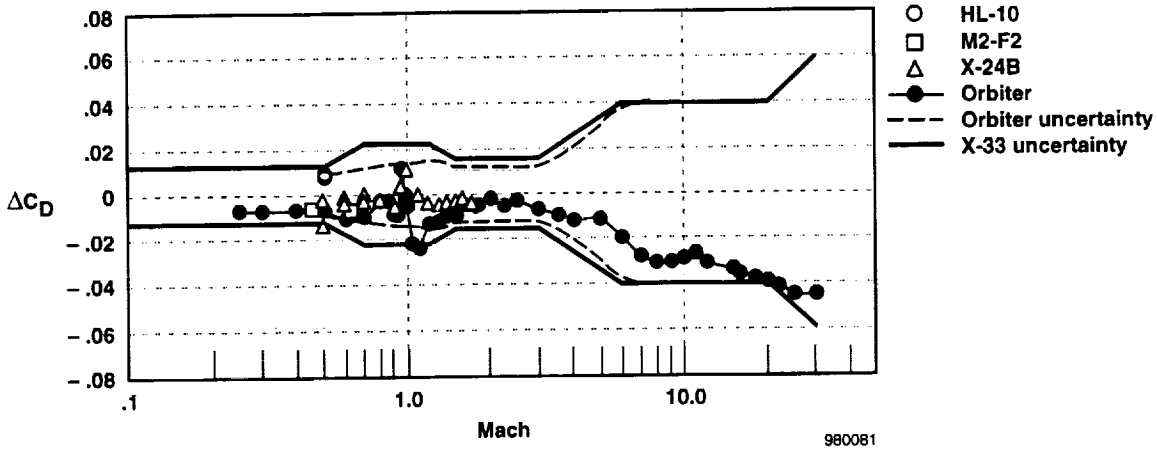

(a) Drag uncertainty.

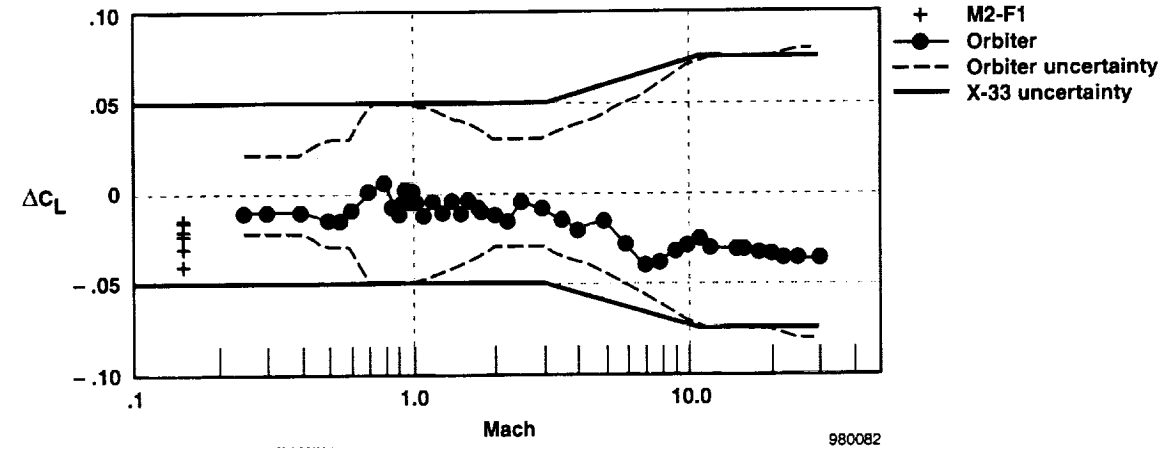

(b) Lift uncertainty.

Figure 5. The X-33 lift and drag uncertainties.

Lift-to-Drag Ratio

Figure 5(c) shows the lift-to-drag ratio variations for the M2-F1, X-24B, and Orbiter vehicles. Based on this sparse amount of data, the recommended X-33 lift-to-drag ratio uncertainties are shown in figure 5(c) and tabulated in table 2. The magnitudes were achieved by increasing the Orbiter uncertainty

20 percent to account for the reduced ground testing expected for the X-33 program. Because lift and drag uncertainties are highly correlated, Romere suggests that the lift-to-drag ratio uncertainty model should be used to limit allowable uncertainties in lift and drag.[15] This limitation prevents the combination lift and drag uncertainty from creating a lift-to-drag ratio dispersion that is more than 3 σ. Figure 6 shows the application of this method. Point A and point B (fig. 6) represent two possible dispersions in lift and drag from the nominal case. In either of these cases, the resulting lift-to-drag ratio remains within the defined uncertainty region (shown shaded). For point C, however, the combined lift and drag uncertainties create a lift-to-drag ratio that is well outside the allowable boundary. In this case, the lift and drag uncertainties should be modified so as not to exceed the lift-to-drag uncertainty boundary limit. Figure 6 shows one method to accomplish this modification. Point C is moved along a line toward the nominal lift and drag until the lift-to-drag ratio is on the uncertainty boundary (point D). The equations used to modify the lift and drag uncertainties are as follows:

$$\Delta C_D = \frac{C_{L_{nom}} - (L/D_{nom} + \Delta L/D_{unc})C_{D_{nom}}}{(L/D_{nom} + \Delta L/D_{unc}) - \dfrac{\Delta C_{L_{unc}}}{\Delta C_{D_{unc}}}} \tag{1}$$

$$\Delta C_L = \frac{\Delta C_{L_{unc}}}{\Delta C_{D_{unc}}}(\Delta C_D) \tag{2}$$

where $C_{L_{nom}}$ is the nominal lift coefficient, $C_{D_{nom}}$ is the nominal drag coefficient, L/D_{nom} is the nominal lift-to-drag ratio, $\Delta C_{L_{unc}}$ is the unmodified lift uncertainty, $\Delta C_{D_{unc}}$ is the unmodified drag uncertainty, L/D_{unc} is the lift-to-drag ratio uncertainty, ΔC_L is the modified lift uncertainty, and ΔC_D is the modified drag uncertainty.

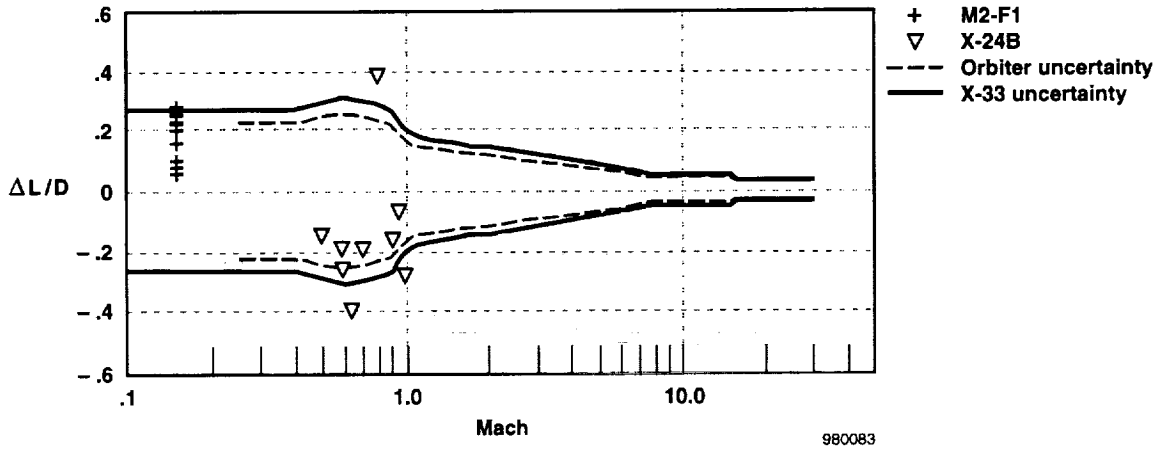

(c) Lift-to-drag ratio.

Figure 5. Concluded.

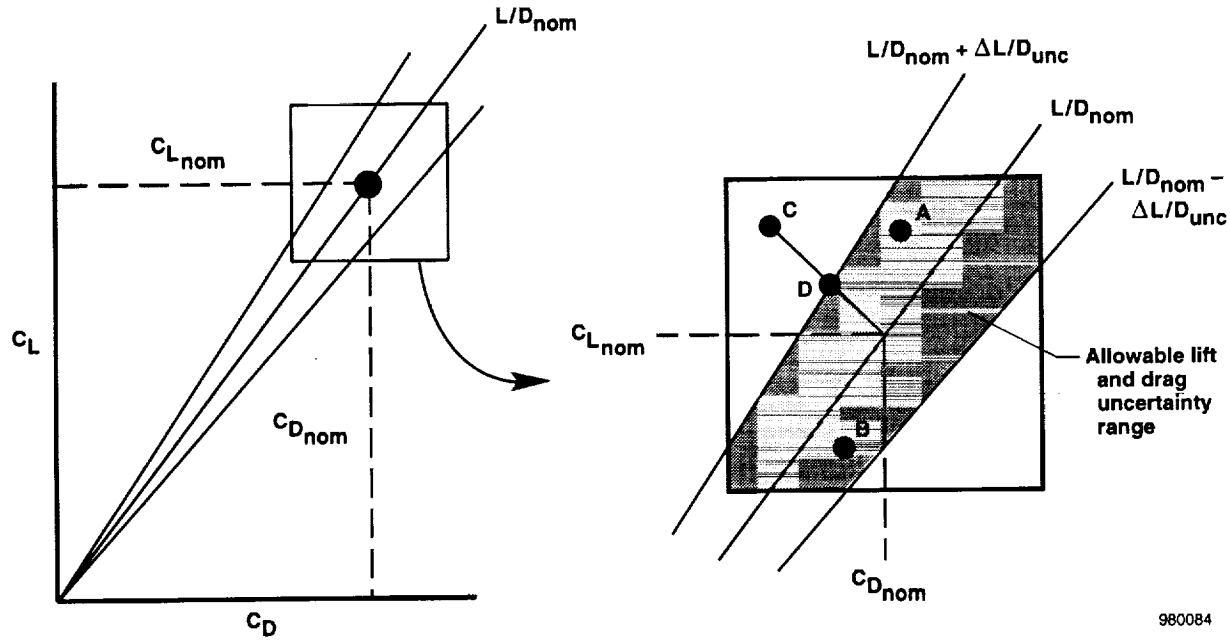

Figure 6. Application of lift and drag aerodynamic uncertainties (see text).

Pitching Moment

Like drag, pitching moment is also susceptible to wind-tunnel measurement errors. The Orbiter had large pitching moment errors at hypersonic speeds caused by real gas effects[16] in addition to the typical variations seen both subsonically and transonically. These real gas effects are reasonably well-understood phenomena that can be estimated through modern computational fluid dynamics codes. For the current X-33 uncertainty model, some attempt is assumed to have been made to account for real gas effects in the aerodynamic model. Without these effects, the uncertainty band should be increased in the hypersonic region. Figure 7 shows the pitching moment prediction errors for the M2-F3, X-24B and Orbiter vehicles. The Orbiter uncertainty bands appear to model the errors well to where the real gas effects begin. Because of the limited wind-tunnel program, some additional uncertainty over the uncertainty modeled by the Orbiter is warranted. The recommended X-33 pitching moment coefficient uncertainty is shown in figure 7 and tabulated in table 3.

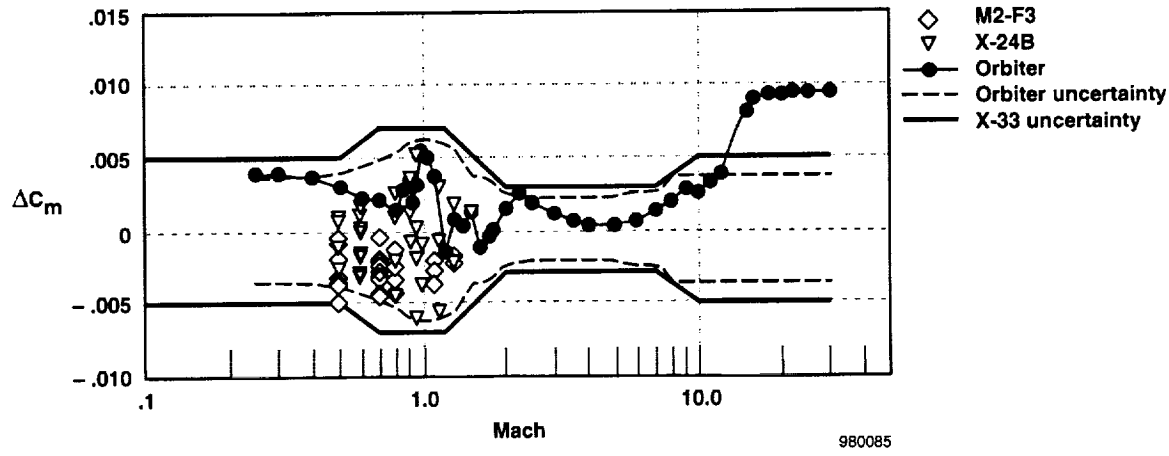

Figure 7. The X-33 pitching moment uncertainty.

Table 3. The X-33 pitching moment, body flap, and elevon uncertainty model.

Mach	ΔC_m	$\Delta C_{m_{\delta bf}}$, percent	$\Delta C_{m_{\delta e}}$, percent
0.10	0.0050	35.0	28.0
0.50	0.0050		
0.70	0.0070		
1.20	0.0070		
2.00	0.0030	35.0	28.0
4.00		43.0	34.4
5.00		43.0	34.4
7.00	0.0030		
8.00		35.0	28.0
10.00	0.0050		
30.00	0.0050	35.0	28.0

Pitch Control Effectiveness

In addition to thrust vectoring, the X-33 vehicle will use body flaps and symmetrical deflection of the elevons to trim the longitudinal axis. Because the body flaps are located in a region with significant separated flow (after main engine cutoff), the uncertainties for the body flap effectiveness would be expected to be higher than a traditional control surface. Figure 6 shows the body flap effectiveness of several lifting bodies and the Orbiter plotted with the Orbiter elevon effectiveness. The Orbiter FAD database shows body flap effectiveness increments as low as one-half of the predicted value at Mach 4.0. In general, the data show an uncertainty variation of 35 percent subsonically and transonically, increasing to approximately 40 percent in the Mach 4.0 region, and diminishing again to 35 percent at greater than Mach 10.0. The recommended X-33 body flap effectiveness coefficient uncertainty is shown in figure 8 and tabulated in table 3. For lack of a better method at the current time, the shape of the body flap effectiveness uncertainty is also used for the elevon control uncertainty. Because the elevons are located outside the base area separated flow field, a reduction in the uncertainty seems warranted. The recommended elevon pitching moment uncertainty, tabulated in table 3, was defined as 80 percent of the body flap uncertainty.

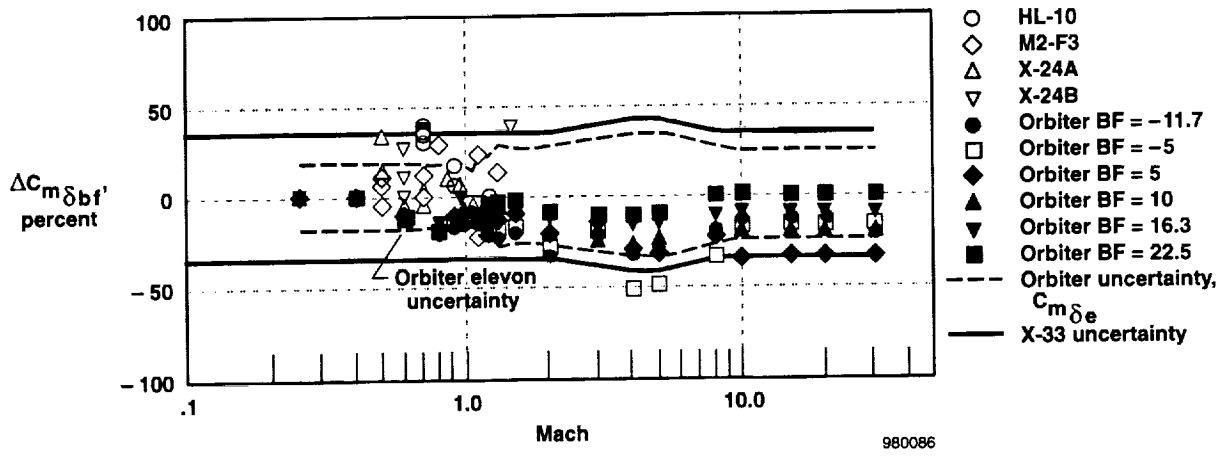

Figure 8. The X-33 body flap pitching moment uncertainty.

Pitch Damping

Figure 7 shows the comparisons of flight test measurements to preflight predictions for pitch damping, C_{m_q}. As previously stated, the plot reflects data points taken from individual flight test maneuvers. As such, maneuver quality and analysis variations add to the magnitude of the scatter. To account for the increased scatter, outliers were discarded in selecting an appropriate uncertainty for the X-33 vehicle. The uncertainty magnitude chosen for the X-33 model (±80 percent) is shown in figure 9 and tabulated in table 4. For C_{m_q}, the preflight prediction codes often underpredicted the amount of damping of the lifting bodies.

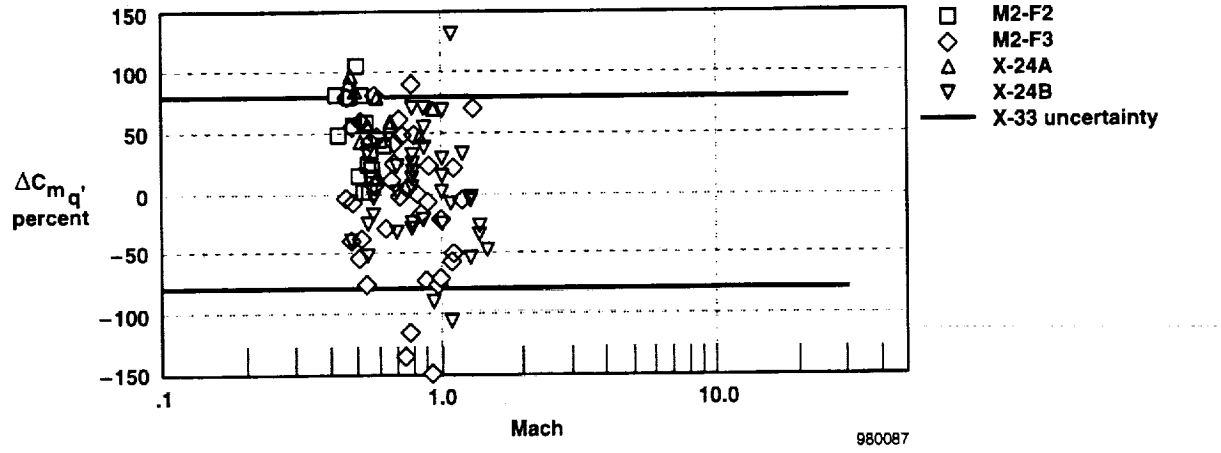

Figure 9. The X-33 pitch damping uncertainty.

Table 4. The X-33 pitch damping uncertainty.

Mach	ΔC_{m_q}, percent
0.1	80.0
30.0	80.0

Lateral-Directional Uncertainties

The lateral-directional derivative uncertainties are discussed in the following subsection. The uncertainty model is composed of effects caused by sideslip, control deflection, and rotation rate.

Sideslip Derivatives

Figure 10(a) shows the derivative errors for rolling moment due to sideslip, ΔC_{l_β}, for the HL-10, M2-F2, M2-F3, X-24A, X-24B, and Orbiter vehicles. The Orbiter uncertainty levels bound the data scatter except for a few outliers. To account for the reduced ground testing expected for the X-33 vehicle, the Orbiter uncertainties were increased by 20 percent. The recommended X-33 dihedral effect uncertainty is shown in figure 10(a) and tabulated in table 5.

Figure 10(b) shows the directional stability, ΔC_{n_β}. The plot clearly shows that the scatter is not evenly distributed around zero. In addition, the Orbiter uncertainty levels do not adequately contain the variation seen on several of the lifting-body programs. The recommended X-33 directional stability uncertainty is shown in figure 10(b) and tabulated in table 5. A nonsymmetrical uncertainty magnitude was selected to better reflect the historical data.

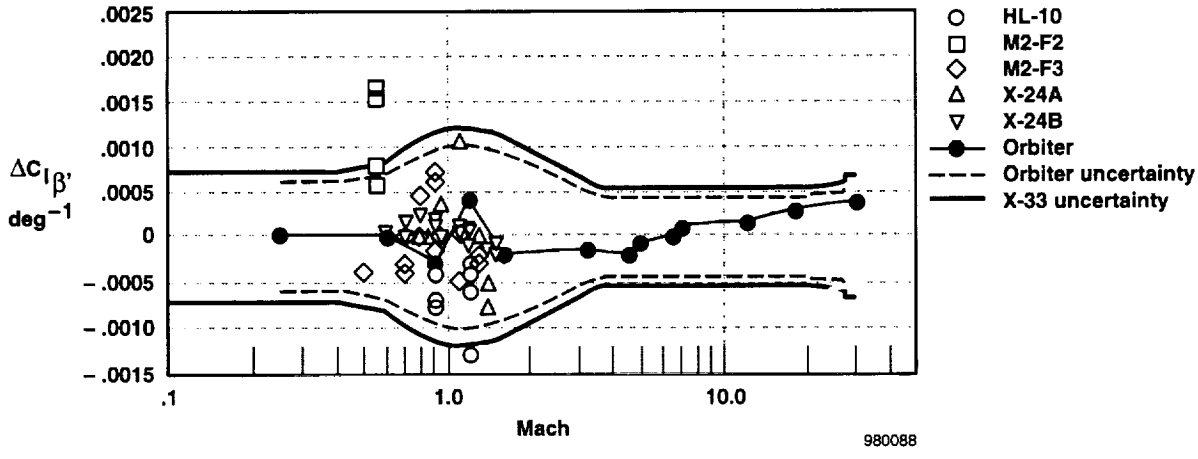

(a) Rolling moment due to sideslip.

Figure 10. The X-33 sideslip derivative uncertainties.

Table 5. The X-33 sideslip derivative uncertainty model.

Mach	ΔC_{l_β}, deg^{-1}	ΔC_{n_β} (+), deg^{-1}	ΔC_{n_β} (–), deg^{-1}	ΔC_{Y_β} (+), deg^{-1}	ΔC_{Y_β} (–), deg^{-1}
0.10	0.00072	0.00070	–0.00070	0.00233	–0.00233
0.40	0.00072	0.00070	–0.00070	0.00233	–0.00233
0.60	0.00084				
0.70		0.00100	–0.00200		
0.80	0.00108			0.00720	–0.00300
0.90	0.00115				
0.95	0.00118			0.00720	
1.05	0.00120			0.00718	
1.10				0.00716	
1.20	0.00120			0.00713	
1.30	0.00119			0.00707	
1.50	0.00114	0.00100	–0.00200	0.00692	
2.00	0.00096	0.00100	–0.00100	0.00636	
3.00	0.00066			0.00526	
3.20	0.00059			0.00506	
3.60	0.00054			0.00469	
4.00				0.00432	
5.00				0.00364	
5.50				0.00359	
8.00		0.00100	–0.00100	0.00336	
9.00		0.00070	–0.00070		
20.00	0.00054			0.00336	
25.00	0.00058	0.00070	–0.00070	0.00480	
30.00	0.00066	0.00090	–0.00090	0.00480	–0.00300

Figure 10(c) shows the derivative errors for the side force due to sideslip, ΔC_{Y_β}. The Orbiter uncertainty levels appear to adequately contain the data variation on the positive side; however, very little data were found showing a negative increment. This asymmetry is similar to the ΔC_{n_β} parameter, which was skewed to the negative direction. The recommended X-33 coefficient uncertainty for side force due to sideslip is shown in figure 10(c) and tabulated in table 5. As with ΔC_{n_β}, a nonsymmetrical uncertainty magnitude was selected to better match the historical data.

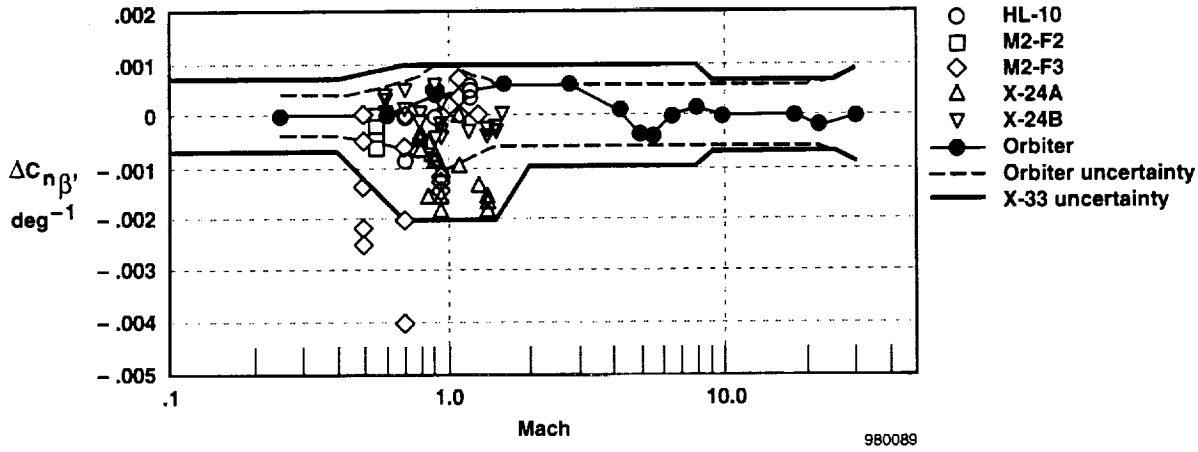

(b) Yawing moment due to sideslip.

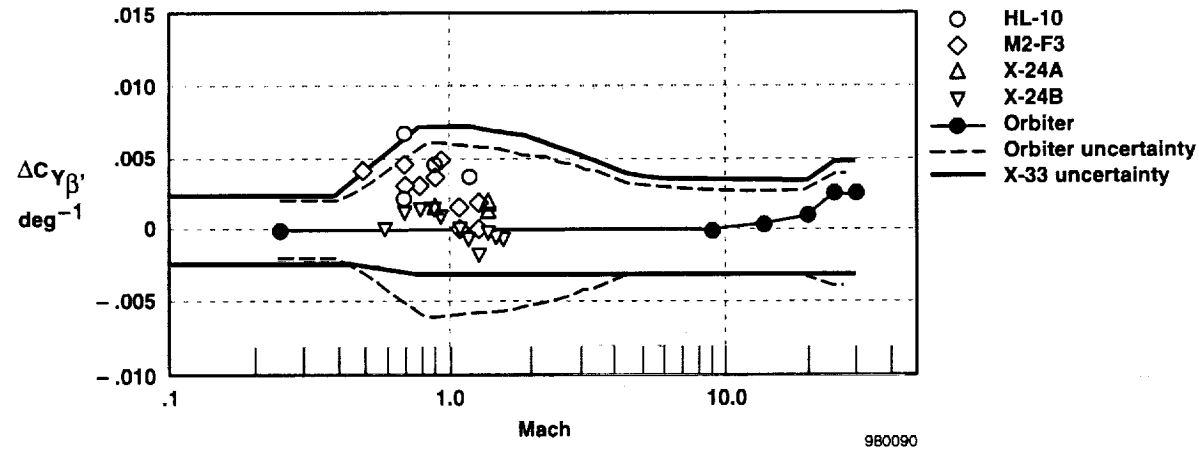

(c) Side force due to sideslip.

Figure 10. Concluded.

Aileron Effectiveness

Figure 11 shows the aileron control derivative variations. Because the Orbiter aileron surface has a much larger moment arm and more control surface area than the lifting-body vehicles, the surface can

generate much larger forces and moments. To minimize this configuration-dependent effect, the rolling moment increments (flight minus prediction) were normalized by the predicted aileron effectiveness. Unfortunately, the derivatives for side force and yawing moment due to aileron achieve small magnitudes, which are not conducive to a normalized comparison. In these cases, the Orbiter uncertainties and FADs were multiplied by a factor that caused the Orbiter uncertainty to be slightly larger than the scatter from the lifting-body data. This uncertainty level was then used as the X-33 uncertainty recommendation. For lack of a better method, the following aileron uncertainties should be used to model the unknowns in the differential body flap and differential elevon control power.

Figure 11(a) shows the roll control power increments, $\Delta C_{l_{\delta a}}$. In this case, the Orbiter uncertainty did not provide a good guide to develop an uncertainty for the X-33 vehicle. The lifting-body data were used in conjunction with the Orbiter FAD to arrive at a roll control power uncertainty. The recommended X-33 roll control power uncertainty is shown in figure 11 and tabulated in table 6.

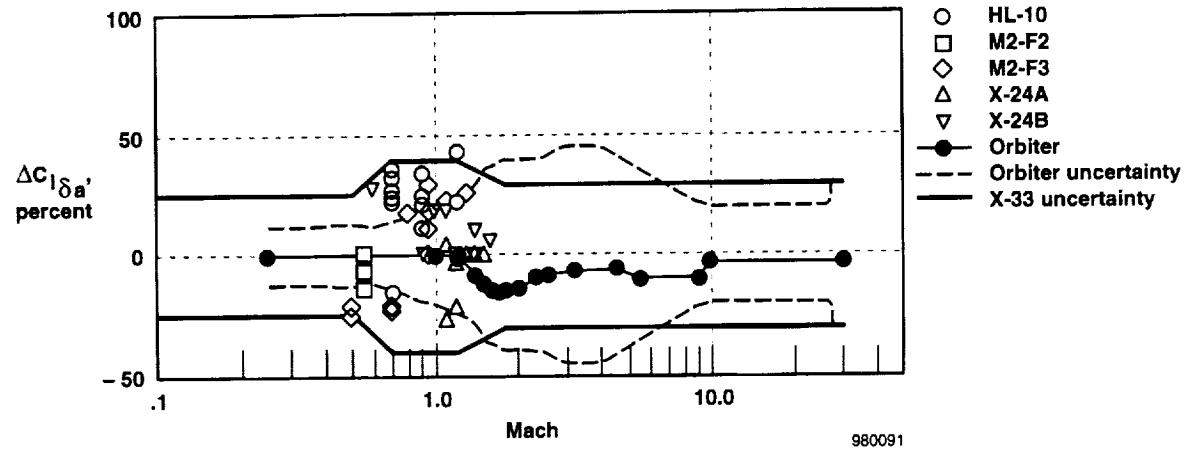

(a) Rolling moment due to aileron.

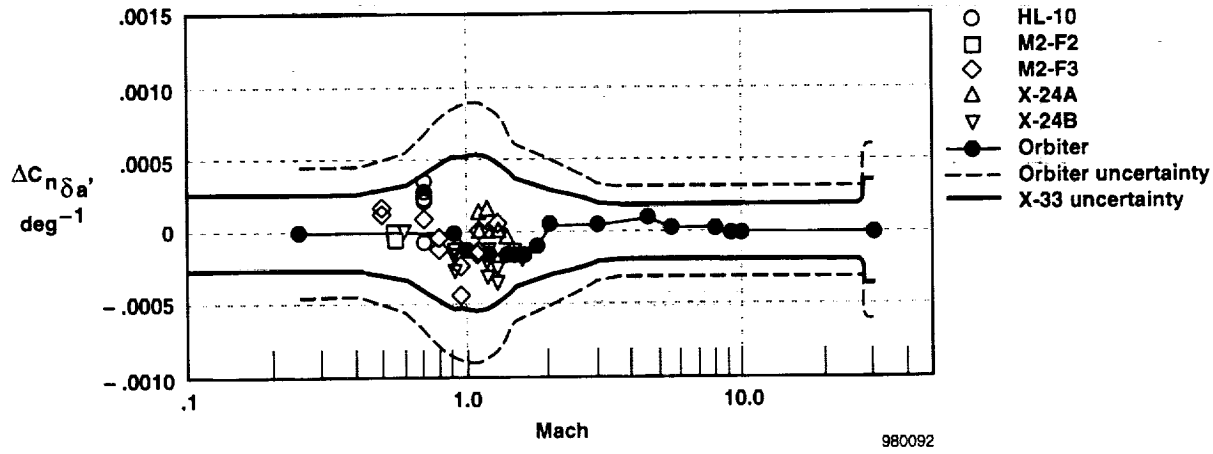

(b) Yawing moment due to aileron.

Figure 11. The X-33 aileron derivative uncertainties.

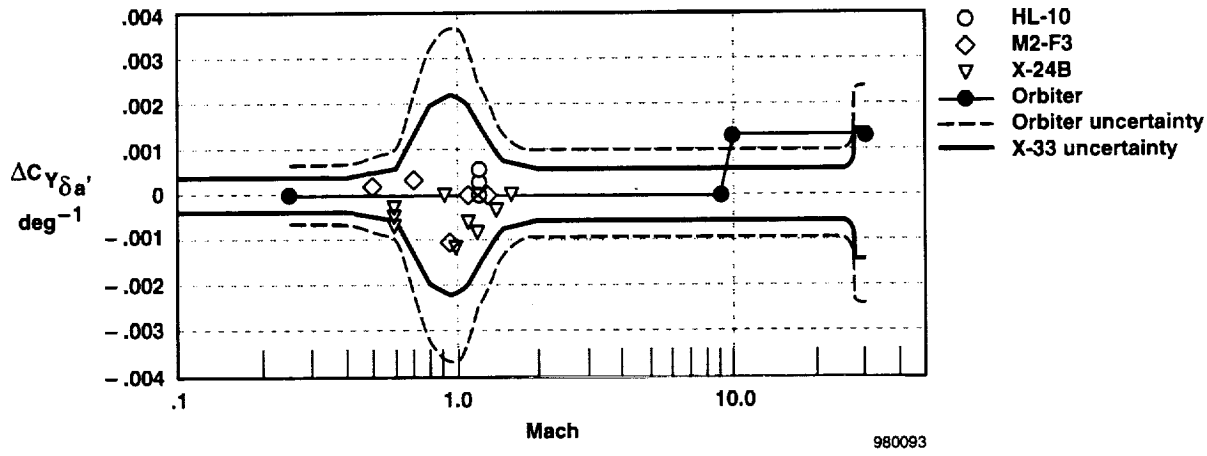

(c) Side force due to aileron.

Figure 11. Concluded.

Table 6. The X-33 aileron derivative uncertainty model.

Mach	$\Delta C_{l_{\delta a}}$, percent	$\Delta C_{n_{\delta a}}$, deg^{-1}	$\Delta C_{Y_{\delta a}}$, deg^{-1}
0.10	25.0	0.00027	0.00039
0.40		0.00027	0.00039
0.50	25.0		
0.60		0.00033	0.00058
0.70	40.0		
0.80		0.00048	0.00198
0.90		0.00052	0.00218
0.95		0.00053	0.00221
1.00		0.00053	
1.05		0.00054	0.00214
1.10		0.00054	0.00198
1.20	40.0	0.00052	0.00149
1.30		0.00048	0.00122
1.40		0.00043	
1.50		0.00037	0.00072

Table 6. Concluded.

Mach	$\Delta C_{l_{\delta a}}$, percent	$\Delta C_{n_{\delta a}}$, deg^{-1}	$\Delta C_{Y_{\delta a}}$, deg^{-1}
1.80	30.0	0.00033	
2.00		0.00030	0.00058
2.20		0.00028	
3.00		0.00020	
4.00		0.00019	
25.35		0.00019	0.00058
26.85		0.00021	0.00072
27.25		0.00026	0.00105
27.35		0.00032	0.00129
27.50		0.00036	0.00144
30.00	30.0	0.00036	0.00144

Figure 11(b) shows increments of the yawing moment due to aileron, $\Delta C_{n_{\delta a}}$. The Orbiter uncertainty was multiplied by 0.6 so that its magnitude was slightly larger than the lifting-body scatter. The recommended X-33 coefficient uncertainty for yawing moment due to aileron is shown in figure 11 and tabulated in table 6.

Figure 11(c) shows increments of the side force due to aileron, $\Delta C_{Y_{\delta a}}$. The Orbiter uncertainty was again multiplied by 0.6 so that its magnitude was slightly larger than the lifting-body scatter. The recommended X-33 coefficient uncertainty for side force due to aileron is shown in figure 11 and tabulated in table 6.

Rudder Effectiveness

The X-33 aircraft has several control effectors for yawing moment generation: thrust vectoring, the vertical tail pair, and asymmetrical deflection of the body flaps. The rudder derivative information shown here from the lifting bodies is based on the large vertical tails present on most lifting bodies. Figure 12 shows the rudder derivative variations.

Figure 12(a) shows increments of the rolling moment due to rudder, $\Delta C_{l_{\delta r}}$. The historical data were sparse because of the difficulty in estimating this particular parameter. The Orbiter uncertainty magnitudes appear to adequately contain the data scatter with enough margin to account for the reduced

ground testing expected for the X-33 vehicle as compared to the Orbiter vehicle. The recommended X-33 coefficient uncertainty for rolling moment due to rudder is shown in figure 12(a) and tabulated in table 7. The X-33 uncertainty magnitude was chosen to be identical to the Orbiter uncertainty.

Table 7. The X-33 rudder derivative uncertainty model.

Mach	$\Delta C_{l_{\delta r}}$, deg^{-1}	$\Delta C_{n_{\delta r}}$, percent	$\Delta C_{Y_{\delta r}}$, deg^{-1}
0.10	0.00016	24.1	0.00150
0.40	0.00016	24.7	
0.50			0.00150
0.60	0.00023	27.4	
0.70			0.00220
0.80	0.00037	31.9	
0.90	0.00041	38.6	
1.00		39.1	
1.20	0.00041	27.5	0.00220
1.30	0.00040	23.8	
1.50	0.00035	23.2	
2.00	0.00024	27.7	0.00120
2.30	0.00021	28.2	
2.60	0.00019	28.5	
2.80		29.6	
3.00	0.00015		
3.20	0.00014	31.8	
3.60	0.00012	35.8	
4.00	0.00010		0.00050
4.20		46.4	
5.00		61.8	
6.00		75.6	
30.00	0.00010	120.0	0.00050

Figure 12(b) shows the rudder control power, $\Delta C_{n_{\delta r}}$. The Orbiter uncertainty appears to bound the lifting-body and Orbiter flight test data. The Orbiter uncertainty was increased by 20 percent to create the recommended X-33 uncertainty. As the Mach number increases to greater than Mach 3, the control power uncertainty increases rapidly. This increase is caused by the increasing angle of attack that blankets the rudder surfaces and sharply reduces their effectiveness. The recommended X-33 rudder control power uncertainty for a reentry trajectory is shown in figure 12(b) and tabulated in table 7. The rudder could possibly be used during the ascent portion of the trajectory, where the angle of attack is small at high Mach numbers. Under these conditions, the rudders will not be blanketed and the uncertainty will not be as large. To account for the lack of a separation wake, the rudder effectiveness uncertainty magnitude is recommended to be maintained at ±30 percent at greater than Mach 3 when angle of attack is less than 10°. The transition between the low and high angle-of-attack database can be made by linearly fading between 10° and 20° angle of attack. This angle-of-attack range corresponds to the range in which the X-33 rudder loses effectiveness at high Mach numbers.

Figure 12(c) shows increments of the side force due to rudder, $\Delta C_{Y_{\delta r}}$. The Orbiter uncertainties do not adequately model the flight data for the lifting bodies. A fairing was drawn to better match the transonic variations seen in lifting-body flight tests and to be somewhat larger than the Orbiter uncertainty in the subsonic and supersonic regions. The recommended X-33 coefficient uncertainty for side force due to rudder is shown in figure 12(c) and tabulated in table 7.

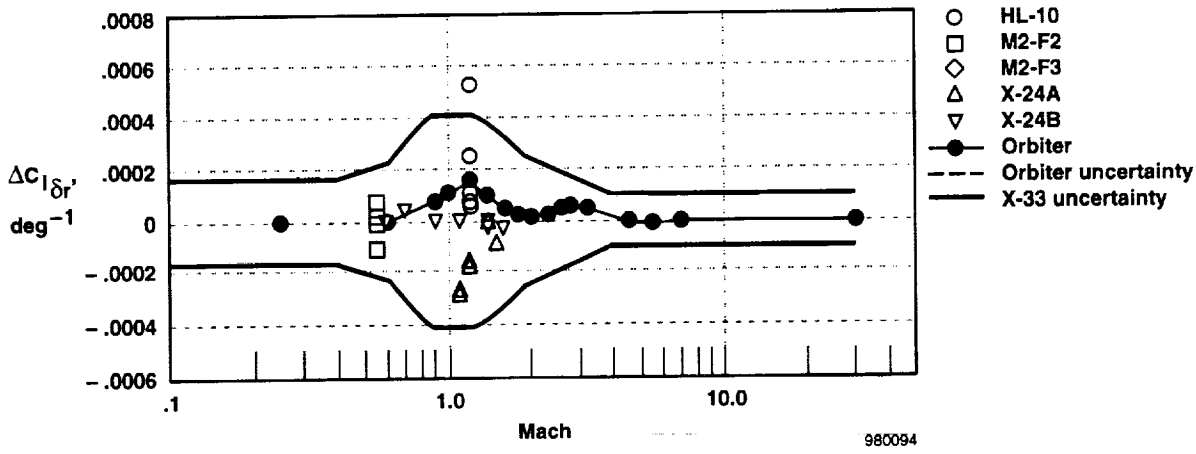

(a) Rolling moment due to rudder.

Figure 12. The X-33 rudder derivative uncertainties.

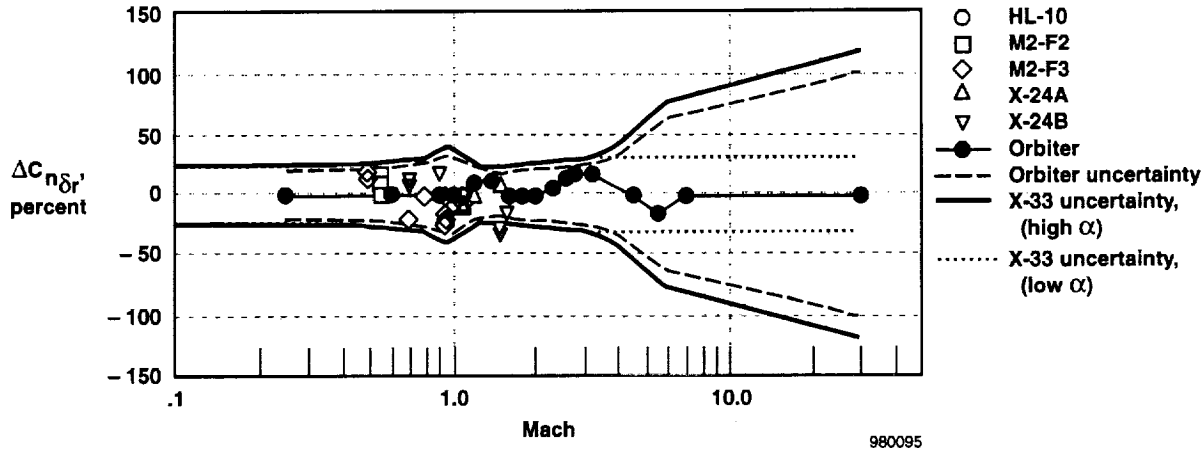

(b) Yawing moment due to rudder.

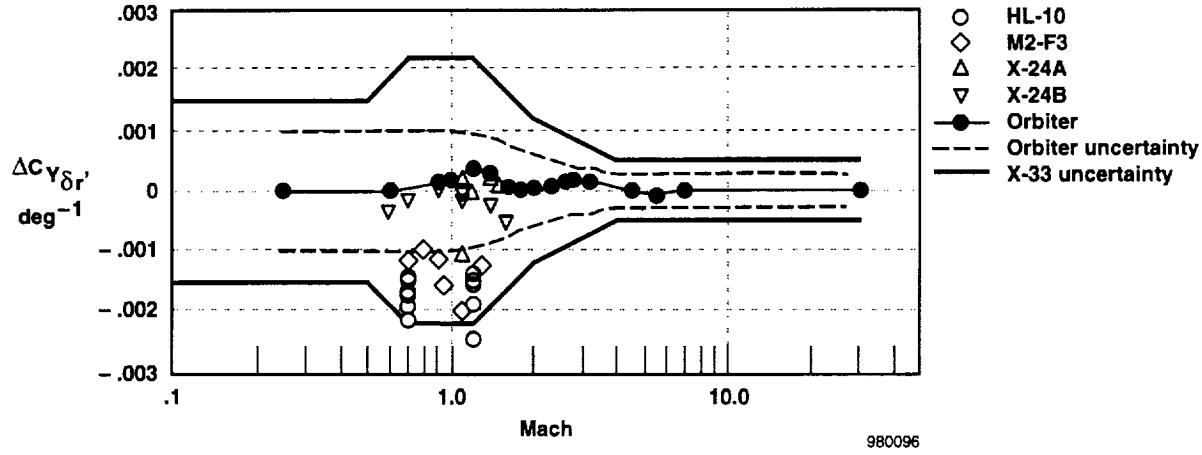

(c) Side force due to rudder.

Figure 12. Concluded.

Rotary Derivatives

Figure 13(a) shows a comparison of flight test estimates to preflight predictions for the roll damping derivative, C_{l_p}. As previously discussed, a large number of the outlier data were neglected for the rotary derivatives because the individual data points, rather than a best fit, were being used for comparison. A majority of the roll damping uncertainty data lie between –40 percent and 70 percent, which were selected as the X-33 uncertainty bounds as shown in figure 13(a) and listed in table 8.

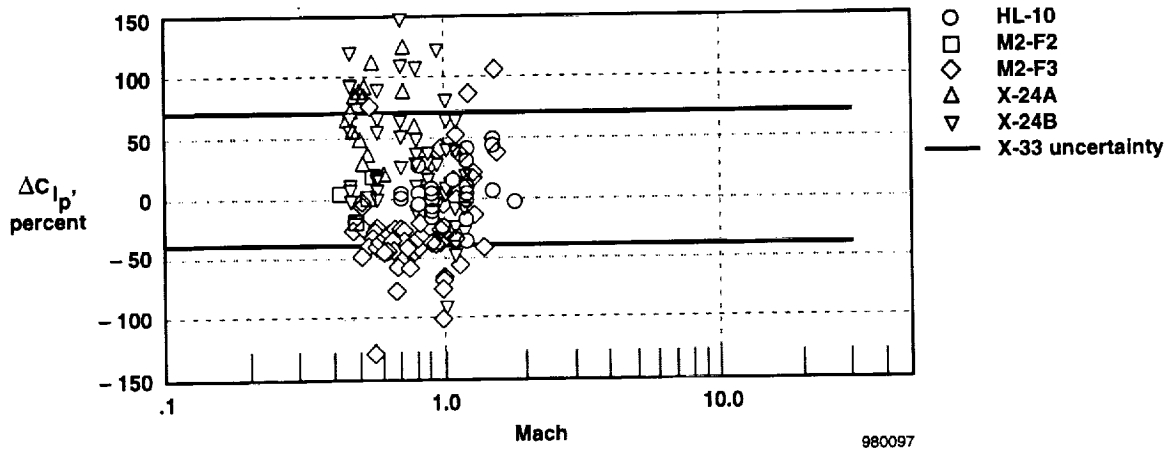

(a) Rolling moment due to roll rate.

Figure 13. The X-33 rolling moment dynamic derivative uncertainties.

Table 8. The X-33 lateral-directional rotary derivative uncertainty model.

Mach	ΔC_{l_p} (–), percent	ΔC_{l_p} (+), percent	ΔC_{l_r} (–), percent	ΔC_{l_r} (+), percent	ΔC_{n_p} (–), percent	ΔC_{n_p} (+), percent	ΔC_{n_r} (–), percent	ΔC_{n_r} (+), percent
0.1	–40.0	70.0	–200.0	150.0	–200.0	100.0	–35.0	40.0
0.8					–200.0	100.0		
0.9					–300.0	200.0		
1.2					–300.0	200.0		
1.5					–200.0	100.0		
30.0	–40.0	70.0	–200.0	150.0	–200.0	100.0	–35.0	40.0

The cross-axis rotary derivatives, C_{l_r} and C_{n_p}, are difficult to predict and difficult to extract from flight data. In addition, the derivatives are usually small, which accentuates any differences seen. In most cases, this accentuation is not a problem because these terms do not often have a significant effect on the vehicle motion. For the X-33 vehicle, however, the cross-axis rotary derivatives can aggravate problems caused by multiaxis control coupling. For example, on the X-33 vehicle, the elevons, body flaps, and rudders each produce pitching, rolling, and yawing moments.

Figure 13(b) shows the rolling moment due to yaw rate uncertainty. The uncertainty data vary over a large range for reasons previously described. The X-33 uncertainty bounds were selected at –200 percent

to 150 percent, which is tabulated in table 8. The X-33 control system must be able to compensate for having the wrong sign on C_{l_r} or having a magnitude 2.5 times higher than predicted.

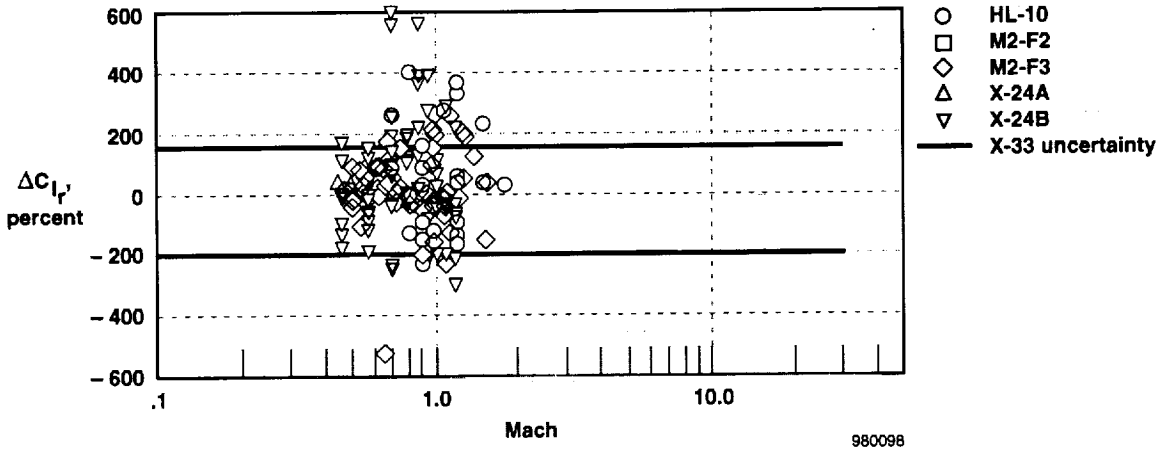

(b) Rolling moment due to yaw rate.

Figure 13. Concluded.

Figure 14(a) shows data for the yawing moment due to roll rate uncertainty. As expected, the scatter is large, increasing through transonic Mach numbers. The X-33 uncertainty bounds were increased in this area to partially account for this effect. The bounds vary from –300 percent to 200 percent transonically and –200 percent to 100 percent subsonically and supersonically. The model is listed in table 8.

Figure 14(b) shows the yawing moment due to yaw rate derivative uncertainty data. As with roll damping, flight results show positive and negative increments of yaw damping. Few data points showed less than one-half the predicted damping. The selected X-33 uncertainty ratio varies from –35 percent to 40 percent, as shown in table 8.

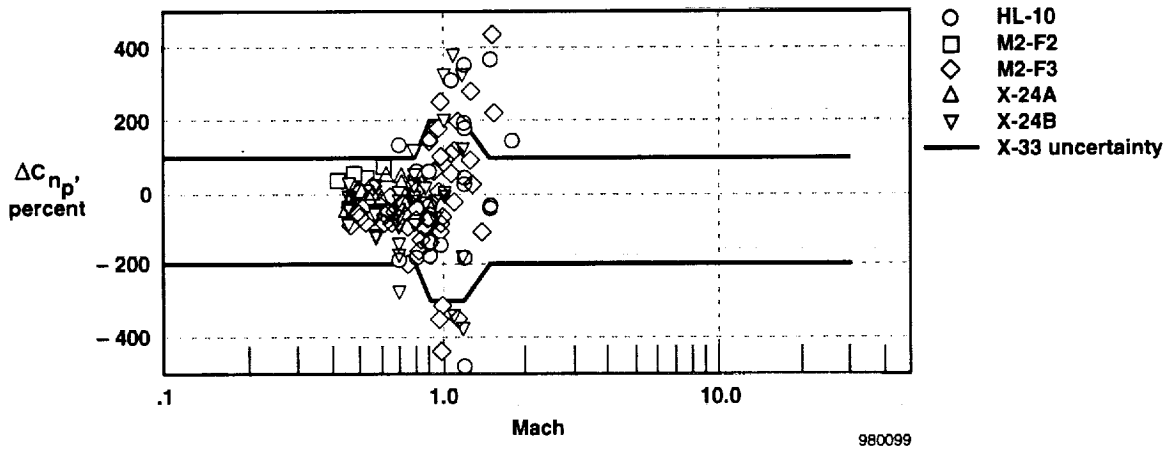

(a) Yawing moment due to roll rate.

Figure 14. The X-33 yawing moment dynamic derivative uncertainty.

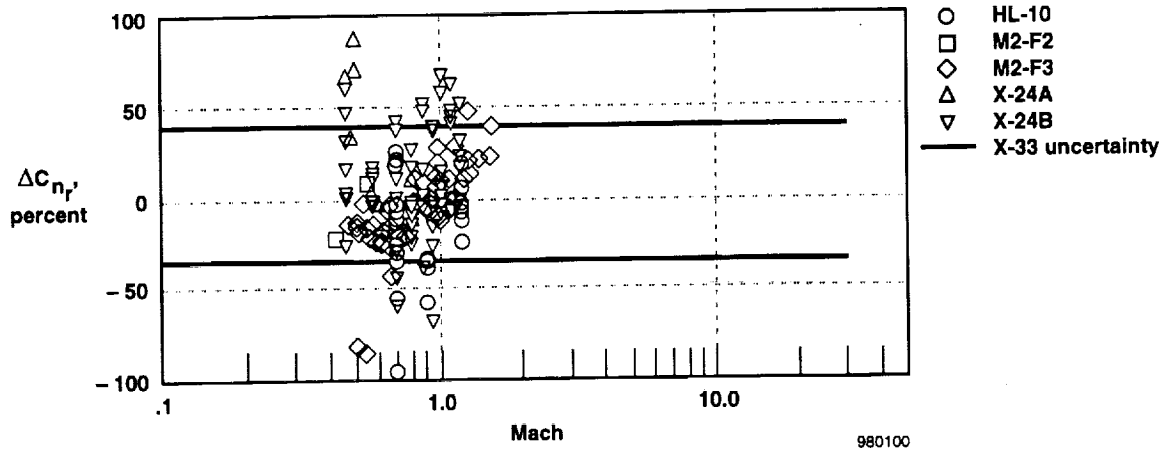

(b) Yawing moment due to yaw rate.

Figure 14. Concluded.

APPLICATION OF UNCERTAINTY MODELS

Now that the aerodynamic uncertainty models have been generated, some method for applying the aerodynamic errors in a logical way must be developed. The X-33 program will employ several types of testing that will use the aerodynamic uncertainty models. These test methods include Monte Carlo simulations of the complete mission and linear analysis of the flight control laws from each of the flight phases. The following subsections will describe some of the details of these two test methods.

Monte Carlo Simulation

Stress testing of the X-33 flight control system would not be complete without simulations of the X-33 missions. This type of testing ensures that adequate margins (control, thermal, structural, and so forth) exist throughout the envelope. The X-33 batch simulation will be used to repeatedly "fly" a specific mission profile. Because the vehicle is completely autonomous, no intervention (by a pilot, for example) is required to simulate a complete flight. This autonomy allows multiple runs with varying aerodynamics to be compared directly.

In order to implement the aerodynamic uncertainty model into a Monte Carlo simulation, the distribution of the uncertainties must be defined. For the X-33 program, the aerodynamic uncertainties were assumed to be normally distributed with the uncertainty magnitudes defined in this paper equivalent to a 3-σ value. This assumption allows the uncertainty magnitudes to be easily scaled to any desired statistical uncertainty value (for example, $2\sigma = (2/3)3\sigma$; $-1\sigma = (-1/3)3\sigma$). For better implementation into the Monte Carlo simulation, the uncertainty models were scaled to 1-σ values. Within the simulation code, the individual 1-σ uncertainty terms are multiplied by normally distributed random numbers, or gains, that have zero mean and unit variance. In order to prevent unreasonable uncertainties, the gains can be limited to a maximum variation (for example, ± 3).

For a given simulation run, each of the aerodynamic uncertainty gains will be randomly set along with the uncertainties gains from other important models, including propulsion, navigation, actuator, RCS, winds, atmosphere, fuel system, and thermal models. Analysis of a statistically significant number of runs will reveal those aerodynamic uncertainty combinations that result in a failure to complete the mission or cause some limit (heating, Mach number, loads, and so forth) to be exceeded. Extreme sensitivity to a particular uncertainty or combination of uncertainties may require an improvement to control law or guidance design. When the flight software is frozen, the Monte Carlo results will be used to show that the mission success criteria (currently 95 percent confidence level for the X-33 program) will be met.

Linear Analysis

The effect of aerodynamic dispersions on the phase and gain margins of the control system will also be assessed. Using the simulation, the X-33 aircraft will be trimmed at points along the trajectories and linear models of the aerodynamics and control system will be output. These models will be used to calculate the phase and gain margins at selected points in the flight envelope.[17] Typically, the criterion for evaluation of the control law is that the control law will be stable when subjected to worst-case uncertainties. Selection of the uncertainty magnitude can be done in a normally random fashion, similar to the Monte Carlo approach described previously; or the important parameters can be perturbed individually (to their maximum uncertainty) or in small groups (to less than their maximum uncertainty).

CONCLUDING REMARKS

An aerodynamic uncertainty model for the X-33 single-stage-to-orbit demonstrator aircraft has been developed. The model is based on comparisons of historical flight test estimates to preflight wind-tunnel and analysis code predictions documented during six lifting-body aircraft and the Space Shuttle Orbiter flight programs. The lifting-body and Orbiter data were used to define an appropriate uncertainty magnitude in the subsonic and supersonic flight regions, and the Orbiter data were used to extend the database to hypersonic Mach numbers. The uncertainty models will be used to perform linear analysis of the X-33 flight control system and Monte Carlo mission simulation studies. The aerodynamic uncertainty models developed herein, along with the uncertainty models of all other systems that affect the vehicle flight characteristics (including propulsion, navigation, actuator, reaction control system, winds, atmosphere, fuel system, and thermal models), will be used to stress-test the autonomous X-33 control and guidance systems. Further refinement of the X-33 aerodynamic uncertainty model may occur at the conclusion of the wind-tunnel test program. Because the aerodynamic uncertainty model was developed exclusively using historical data rather than X-33 specific characteristics, the model may be useful to other lifting-body studies.

REFERENCES

[1]Young, James C. and Jimmy M. Underwood, "The Development of Aerodynamic Uncertainties for the Space Shuttle Orbiter," *Shuttle Performance: Lessons Learned,* NASA CP-2283, Part 2, 1983, pp. 1169–1185.

[2]Weil, Joseph and Bruce G. Powers, *Correlation of Predicted and Flight Derived Stability and Control Derivatives—With Particular Application to Tailless Delta Wing Configurations,* NASA TM-81361, 1981.

[3]Pyle, Jon S., *Lift and Drag Characteristics of the HL-10 Lifting Body During Subsonic Gliding Flight,* NASA TN-D-6263, 1971.

[4]Strutz, Larry W., *Flight-Determined Derivatives and Dynamic Characteristics for the HL-10 Lifting Body Vehicle at Subsonic and Transonic Mach Numbers,* NASA TN-D-6934, 1972.

[5]Horton, Victor W., Richard C. Eldredge, and Richard E. Klein, *Flight-Determined Low-Speed Lift and Drag Characteristics of the Lightweight M2-F1 Lifting Body,* NASA TN-D-3021, 1965.

[6]Kempel, Robert W. and Ronald C. Thompson, *Flight-Determined Aerodynamic Stability and Control Derivatives of the M2-F2 Lifting Body Vehicle at Subsonic Speeds,* NASA TM-X-2413, 1971.

[7]Pyle, Jon S. and Robert H. Swanson, *Lift and Drag Characteristics of the M2-F2 Lifting Body During Subsonic Gliding Flight,* NASA TM-X-1431, 1967.

[8]Sim, Alex G., *Flight-Determined Stability and Control Characteristics of the M2-F3 Lifting Body Vehicle,* NASA TN-D-7511, 1973.

[9]Kirsten, Paul W., "Wind Tunnel and Flight Test Stability and Control Derivatives for the X-24A Lifting Body," FTC-TD-71-7, Apr. 1972.

[10]Nagy, Christopher J. and Paul W. Kirsten, "Handling Qualities and Stability Derivatives of the X-24B Research Aircraft," AFFTC-TR-76-8, Mar. 1976.

[11]Richardson, David F., "Comparison of Flight Test and Wind Tunnel Performance Characteristics of the X-24B Research Aircraft," AFFTC-TR-76-10, Apr. 1976.

[12]Sim, Alex G., *A Correlation Between Flight Determined Derivatives and Wind-Tunnel Data for the X-24B Research Aircraft,* NASA TM-113084, 1997.

[13]Iliff, Kenneth W. and Mary F. Shafer, *Extraction of Stability and Control Derivatives From Orbiter Flight Data,* NASA TM-4500, 1993.

[14]Rockwell International, "Operational Aerodynamic Data Book," Volume 3, STS85-0118 CHG3, Mar. 1991.

[15]Romere, Paul O., "STS-26 Flight Assessment Package (FAD 26): Orbiter Aerodynamics," JSC Report 22078, Apr. 1986.

[16]Maus, J. R., B. J. Griffith, K. Y. Szema, and J. T. Best, "Hypersonic Mach Number and Real Gas Effects on Space Shuttle Orbiter Aerodynamics," AIAA-83-0343, Jan. 1983.

[17]Bosworth, John T., *Linearized Aerodynamic and Control Law Models of the X-29A Airplane an Comparison With Flight Data*, NASA TP-4356, 1992.

REPORT DOCUMENTATION PAGE

Form Approved
OMB No. 0704-0188

1. AGENCY USE ONLY (Leave blank)	2. REPORT DATE	3. REPORT TYPE AND DATES COVERED
	April 1998	Technical Paper

4. TITLE AND SUBTITLE

Development of the X-33 Aerodynamic Uncertainty Model

5. FUNDING NUMBERS

WU 242 33 02 00 23 00 TA2

6. AUTHOR(S)

Brent R. Cobleigh

7. PERFORMING ORGANIZATION NAME(S) AND ADDRESS(ES)

NASA Dryden Flight Research Center
P.O. Box 273
Edwards, California 93523-0273

8. PERFORMING ORGANIZATION REPORT NUMBER

H-2221

9. SPONSORING/MONITORING AGENCY NAME(S) AND ADDRESS(ES)

National Aeronautics and Space Administration
Washington, DC 20546-0001

10. SPONSORING/MONITORING AGENCY REPORT NUMBER

NASA/TP-1998-206544

11. SUPPLEMENTARY NOTES

12a. DISTRIBUTION/AVAILABILITY STATEMENT

Unclassified—Unlimited
Subject Category 02

12b. DISTRIBUTION CODE

13. ABSTRACT (Maximum 200 words)

An aerodynamic uncertainty model for the X-33 single-stage-to-orbit demonstrator aircraft has been developed at NASA Dryden Flight Research Center. The model is based on comparisons of historical flight test estimates to preflight wind-tunnel and analysis code predictions of vehicle aerodynamics documented during six lifting-body aircraft and the Space Shuttle Orbiter flight programs. The lifting-body and Orbiter data were used to define an appropriate uncertainty magnitude in the subsonic and supersonic flight regions, and the Orbiter data were used to extend the database to hypersonic Mach numbers. The uncertainty data consist of increments or percentage variations in the important aerodynamic coefficients and derivatives as a function of Mach number along a nominal trajectory. The uncertainty models will be used to perform linear analysis of the X-33 flight control system and Monte Carlo mission simulation studies. Because the X-33 aerodynamic uncertainty model was developed exclusively using historical data rather than X-33 specific characteristics, the model may be useful for other lifting-body studies.

14. SUBJECT TERMS

Aerodynamic uncertainty, Lifting-body aircraft, Monte Carlo simulation, Reusable Launch Vehicle, Stability and control derivatives, X-33

15. NUMBER OF PAGES

39

16. PRICE CODE

A03

17. SECURITY CLASSIFICATION OF REPORT	18. SECURITY CLASSIFICATION OF THIS PAGE	19. SECURITY CLASSIFICATION OF ABSTRACT	20. LIMITATION OF ABSTRACT
Unclassified	Unclassified	Unclassified	Unlimited